Hindawi
Journal of Nanotechnology
Volume 2018, Article ID 3250932, 23 pages
https://doi.org/10.1155/2018/3250932

Review Article

Nanobismuth: Fabrication, Optical, and Plasmonic Properties—Emerging Applications

Ye Tian[1] **and Johann Toudert**[2]

[1]*School of Communication and Electronics Engineering, Hunan City University, Yiyang 413000, China*
[2]*Laser Processing Group (LPG), Instituto de Óptica, CSIC, Madrid, Spain*

Correspondence should be addressed to Ye Tian; tianye-man@163.com

Received 8 December 2017; Accepted 11 April 2018; Published 6 June 2018

Academic Editor: Paresh Chandra Ray

Along the twentieth century, the electronic properties of bismuth have been widely studied, especially in relation with its magnetoresistive and thermoelectric responses. In this context, a particular emphasis has been made on electronic confinement effects in bismuth nanostructures (or nanobismuth). In the recent years, the optical properties of bismuth nanostructures are focusing a growing interest. An increasing number of reports point at the potential of such nanostructures to support plentiful optical resonances over an ultrabroad spectral range: "interband plasmonic" resonances in the ultraviolet, visible, and near-infrared; dielectric Mie resonances in mid- and far-infrared; and conventional free-carrier plasmonic resonances in the far-infrared and terahertz. With the aim to provide a comprehensive basis for exploiting the full optical potential of bismuth nanostructures, we review the current progress in their controlled fabrication, the trends reported (from theoretical calculations and experimental observations) for their optical and plasmonic response, and their emerging applications, including photocatalysis and switchable metamaterials.

1. Introduction

Optical resonances in nanostructures much smaller than the wavelength of light have attracted a broad attention because they allow operating light in small dimensions, for example, allowing efficient harvesting or confinement at the nanoscale [1]. The wavelength of the resonances can be tuned in a static way, by properly engineering the nanostructure composition, shape and size, or a dynamic way through changes in the surrounding medium (its temperature, refractive index, illumination, and so on) [1–7].

Nowadays, a wide range of optically resonant nanostructures rely on the excitation of surface plasmons, that is, the collective oscillations of free charge carriers. Based on the surface plasmon resonances that develop in noble metal nanostructures (Ag and Au) [1, 2], in the visible and near-infrared, amounts of applications, including surface-enhanced Raman scattering (SERS), photothermal therapy, biosensing, hot carrier generation for photovoltaic conversion, and quantum information processing [8–13], have been demonstrated over the last decades. Since then, surface plasmon resonances have been achieved with "alternative" plasmonic materials, for example, other metals (Al, Pt, and Pd) [14, 15], transparent conductive oxides [16], metal nitrides [17], doped semiconductors [16], and graphene [18]. Such materials display a plasmonic response in different spectral regions, as dictated by their free charge carrier density N. Note that plasmonic resonances can be excited when the complex dielectric function of the material ($\varepsilon = \varepsilon_1 + i\varepsilon_2$) shows suitable values, especially having a negative real part ($\varepsilon_1 < 0$) is required. Note also that such conditions can be fulfilled without the need of free-carrier excitation, for instance at the high energy side of the strong interband transitions of some p-block elements, allowing the so-called "interband plasmonic" resonances [19].

Bismuth (Bi), as a fantastic p-block semimetal with highly anisotropic Fermi surface, small effective electron mass, low carrier density, and long carrier mean-free path [20–23], is conventionally deemed as a sound candidate to observe and investigate quantum confinement and finite-size effects, enhanced magnetoresistance, and thermoelectricity [21, 22, 24, 25]. In contrast to the very strong interest in the electrical properties of bismuth, its optical response

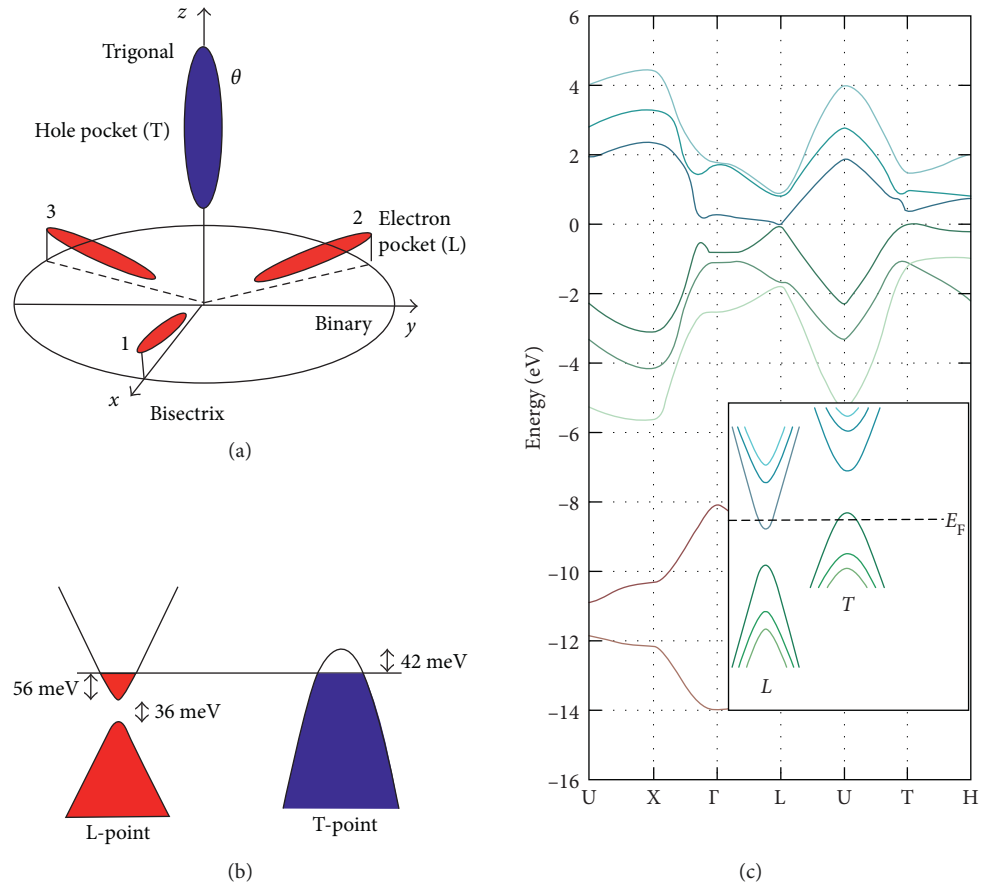

FIGURE 1: (a) Brillouin zone of bismuth (Bi) in the momentum space: one hole pocket at the T-point and three electron pockets at the T-point. (b) Electronic band structure of Bi near the Fermi level [29, 30]. At room temperature, the direct bandgap at the L-point has an energy of 36 meV, the electron Fermi energy at the L-point is 56 meV, and the hole Fermi energy at the T-point is 42 meV. (c) Full band diagram of Bi calculated by the third-neighbor tight-bonding model accounting for the spin-orbit coupling. Reprinted from [31] © 2015 Fuseya et al., originally published in *Journal of the Physical Society of Japan*, vol. 84, p. 012001, 2015, doi: 10.7566/JPSJ.84.012001, under CC by 4.0 license.

has been less studied over the past. Few works reported the optical properties of bulk Bi and Bi thin films and even less for Bi nanostructures (or "nanobismuth"). Very recently, Bi has become increasingly attractive mostly due to the potential of its nanostructures to support optical resonances in the ultraviolet (UV), visible (Vis), and near-infrared (near-IR) regions. It has been proposed that such resonances have an "interband plasmonic" origin. Besides, a "traditional" free-carrier-based plasmonic response is expected in the far-IR to terahertz (THz), and dielectric Mie resonances have been recently predicted in the mid-IR to far-IR region. Moreover, along with the theoretical and experimental studies on the optical response of Bi nanostructures, their potential for emerging applications, such as switchable metamaterials or photocatalysis [7, 26], are also being explored. In this review paper, we summarize the advances in the field of the optical and plasmonic properties of Bi nanostructures over the last years. After a synthetic presentation of the optoelectronic properties of bulk Bi, we review the progress in the fabrication of Bi nanostructures, in the theoretical calculations and experimental observations of their optical and plasmonic responses, and the works about the related emerging applications. Such a review will help to assess the potential of nanobismuth as a new material for plasmonics and nanophotonics with ultrabroad spectral response from the UV to THz region.

2. Optoelectronic Properties of Bulk Bismuth

2.1. Electronic Band Structure. Bi is a semimetal with unique physical properties, including long charge carrier mean-free path (~1 micron at room temperature) [27], huge magnetoresistance [24], or quantum confinement effects in nanostructures with dimensions of tens of nanometers [28]. Such peculiar features originate from the peculiar electronic band structure of the rhombohedral Bi, which presents a highly anisotropic Brillouin zone [29]. Such an anisotropy is exemplified in Figure 1(a) [29], which illustrates the existence of different carrier pockets depending on the spatial direction. Near the T-point of the Brillouin zone, Bi has one hole pocket (hole Fermi surface (FS), aligned ellipsoidically with the trigonal axis z). Near the three equivalent L-points, there are three identical electron pockets (electron FS ellipsoids arrayed symmetrically around the hole FS with a small tilted angle

(~6.5°) out of the plane defined by the bisectrix and binary axes). These three equivalent L-points have both conduction and valence bands, separated by a small bandgap of 36 meV at room temperature (Figure 1(b)) [30, 31]. The Fermi level is located in the conduction band at the L-point and in the valence band at the T-point: this produces semimetallic characteristics where electrons and holes coexist, as shown in Figure 1(b). As a consequence of this semimetal character, Bi presents a very low free-carrier density (N_{Bi}, in the range from 10^{18} to 10^{19} cm^{-3}).

Beyond this semimetallic character that arises from the electronic band structure near the Fermi level, it is worth mentioning that Bi has a rich variety of lower-lying energy bands as demonstrated in the band diagram of bismuth (Figure 1(c)), which have been predicted early theoretically [32, 33] and probed by photoelectron or optical spectroscopy. As we will see below, electronic transitions from lower-lying energy bands can be probed optically in the UV, Vis, and IR regions, whereas the free charge carriers involved in the semimetallic conduction of Bi can be probed only with far-IR and THz light. Indeed, optical absorption by the free charge carriers of Bi becomes relevant in the far-IR-THz regions, owing to their low plasma energy $E_{p,Bi} = h\sqrt{(N_{Bi}e^2/4\pi^2 m\varepsilon_0)} \approx 0.05$ eV that results from the very small value of N_{Bi}.

2.2. The Optical Dielectric Function of Bulk Bismuth. Although Bi is an interesting element with a rich electronic band structure that impacts its optical response, as discussed in Section 2.1, the optical properties of Bi have been less explored than the electronic ones [24, 28, 29]. Especially, the optical dielectric function $\varepsilon = \varepsilon_1 + i\varepsilon_2$ of bulk Bi was reported early by several authors, but in limited spectral regions, and shows a broad dispersion (related mostly with a limited sample quality) as seen in Figure 2. It is only recently that works providing a refined optical characterization of Bi crystals and films were reported [33–35]. Especially, a systematic spectroscopic ellipsometry characterization from the far-IR to the UV was performed on high quality Bi films to provide an artefact-free and Kramers–Kronig consistent dielectric function of the Bi material [19]. In this work, only the dielectric function standing for the in-plane response of the films (i.e., perpendicular to the trigonal axis) was determined. Yet, although the dielectric function of Bi crystals along the trigonal axis has been probed early in the near- to mid-IR showing no marked optical anisotropy in this region, it remains to be measured accurately in a broader spectral region (discussion and related references in [35]).

From the dielectric function shown in Figure 2, it is seen that $\varepsilon_1 < 0$ in the UV, visible, and near-IR regions, thus allowing a plasmonic response in this region. It has been shown in [35] that such negative ε_1 originates from the strong interband transitions peaking at 0.8 eV, whereas the negative ε_1 in the far-IR and THz originates from the free-carrier contribution. In sum, Bi nanostructures have the potential to display plasmonic effects in two spectral regions: (i) in the far-IR and THz due to the collective excitation of free carriers and (ii) in the UV-Vis-near-IR regions where, unlike the conventional plasmonic resonances of noble metals driven by the collective excitation of free electrons, the resonances in Bi nanostructures would be totally induced by interband transitions and called "interband plasmonic" resonances [19]. Furthermore, in between these two plasmonic regions, ε_1 takes very high positive values, thus making Bi an interesting candidate for supporting dielectric Mie resonances in nanostructures at mid- and far-infrared wavelengths.

3. The Growth of Nanobismuth

Amounts of Bi nanostructures have been successfully prepared: 0D nanostructures (including nanoparticles, nanospheres, and nanocubes), 1D nanostructures (including nanowires, nanorods, and nanotubes), and 2D nanostructures (including nanoplates, nanosheets, and thin or ultrathin films), with continuously improved crystalline quality [36–58]. The size of these structures covers the range from a few atoms to few microns, which has allowed a wide suitability for studies in various fields including quantum transport, thermoelectricity, topological insulators, giant magnetoresistance, and superconductivity [24, 59–62]. Such size control is also especially relevant for the fields of plasmonics and nanophotonics, where the working wavelength of the system is closely related to the dimension of the nanostructures. The wide size range of the existing Bi nanostructures would thus provide abundant building blocks to construct optical systems suitable for different wavelength ranges from the UV region to the far-IR and THz regions [34, 35, 63–65].

As the precondition of the studies to the properties of nanobismuth, its fabrication methods were explored intensively over the past few years. They can be divided into two groups: one is template based, where selected matrices are used to prepare the Bi nanostructures [60, 66–70], and the other is template free. In the latter case, many techniques are used. Stress effects are quite useful for fabricating the Bi nanowires [27, 71]. Physical vapor deposition (PVD, mainly RF sputtering and thermal evaporation) has demonstrated its potential for the mass production of Bi nanowires and nanorods, as well as tilted Bi nanocolumns [39, 40, 42]. Solution-phase synthesis allows fabrication of Bi nanostructures with a wide control in their shape, either for 0D, 1D, and 2D nanostructures [24, 45–48, 54, 58, 72, 73]. Laser-induced approaches have been successfully used to produce Bi thin films, nanorods, and nanoparticles [34, 35, 43, 51, 63]. Molecular beam epitaxy (MBE), electron-beam lithography (EBL), electron-beam irradiation, electromigration (EM), and plasma force have also been used [53, 57, 62, 74]. In the following, these methods will be discussed one after another.

3.1. Template-Based Method. Template-based methods used for growing Bi nanostructures rely mostly on the use of anodized aluminium oxide (AAO) templates, which serve as the host material with a uniform porous structure, as shown in Figure 3(a) [75]. By tuning the anodization parameters, the pore diameter and packing density of AAO can be well controlled [67, 75]. In such AAO templates, arrays of Bi nanowires were grown by filling the pores by pressurized injection of liquid Bi (the liquid-phase method), by

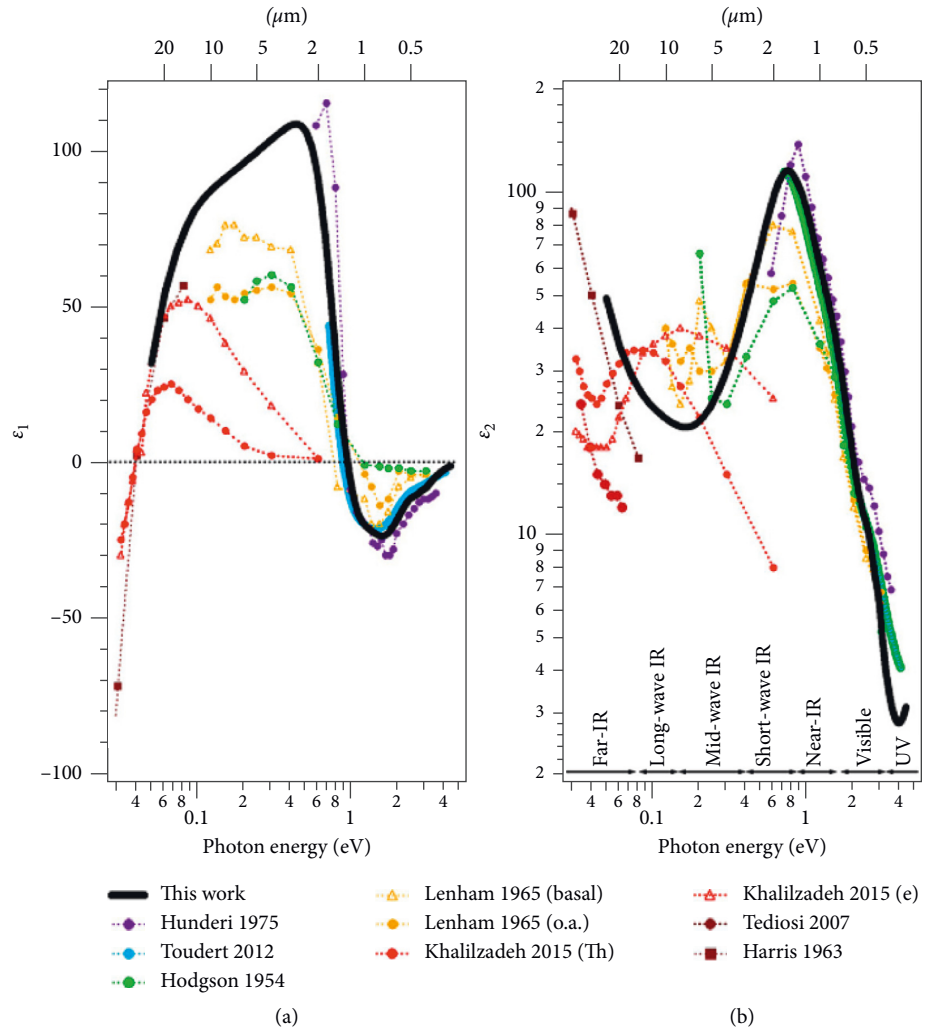

FIGURE 2: Broadband dielectric function ($\varepsilon = \varepsilon_1 + i\varepsilon_2$, black) of bulk Bi together with literature data, showing their broad dispersion. The origin of these data and the reasons behind their dispersion (mostly in relation with the sample quality) are discussed in [34, 35]. Reprinted with permission from American Chemical Society.

electrochemical deposition, or by vapor-phase deposition, as shown in Figures 3(b)–3(e) [60, 67, 68]. Using pressurized injection, most Bi nanowires could be single crystalline along the [202] direction in the hexagonal lattice with a broad diameter tunability range (12–109 nm), but they experience high stress [75]. If using the electrochemical or vapor-phase deposition methods, the nanowire diameter could be further reduced to 7 nm [20]. Moreover, upon rational choice of the parameters for electrochemical deposition, Bi nanotubes can also be prepared (Figure 3(f)) [76]. The main drawbacks of the AAO template methods are the small aspect ratio and surface irregularities of the fabricated nanowires or nanotubes. Moreover, due to the difficulty in removing the AAO and subsequently extracting individual nanowires or nanotubes [76–78], the characterization of samples based on the AAO templates provided mostly ensemble measurements over the whole array. Also, in these cases, the influence of the AAO on the macroscopic properties of the sample is hard to be subtracted.

Unlike the AAO template method, the Ulitovsky method can be used to obtain individual nanowires [68, 70]. It involves a two-step process. Firstly, Bi is inserted in a borosilicate glass capsule where it is heated by a high-frequency induction coil. Secondly, the softened capsule as well as the molten Bi within (note that the melting temperature of bulk Bi is only 271°C) is drawn out by spooling. This method can produce ultralong single-crystalline Bi nanowires along [111] direction in a conventional hexagonal lattice system with diameter down to 55 nm, as shown in Figure 4(a) [70]. Moreover, the surface oxidization to the nanowires can be avoided since in this process the molten Bi is not air-exposed [41]. The optical transparency of the glass is interesting for nanophotonics or plasmonics studies.

Quartz can also serve as a template, upon digging holes using optical fibers, following a method comparable with that applied in the manufacture of hollow-core photonic crystal fibers [79]. Hence, similarly with the pressurized injection process that is used with AAO templates [75], the molten Bi can be injected into the holes of the quartz templates where the Bi nanowires form (Figure 4(b)) [80]. Although the quartz template method has several benefits, such as achievable nanowire lengths comparable with the

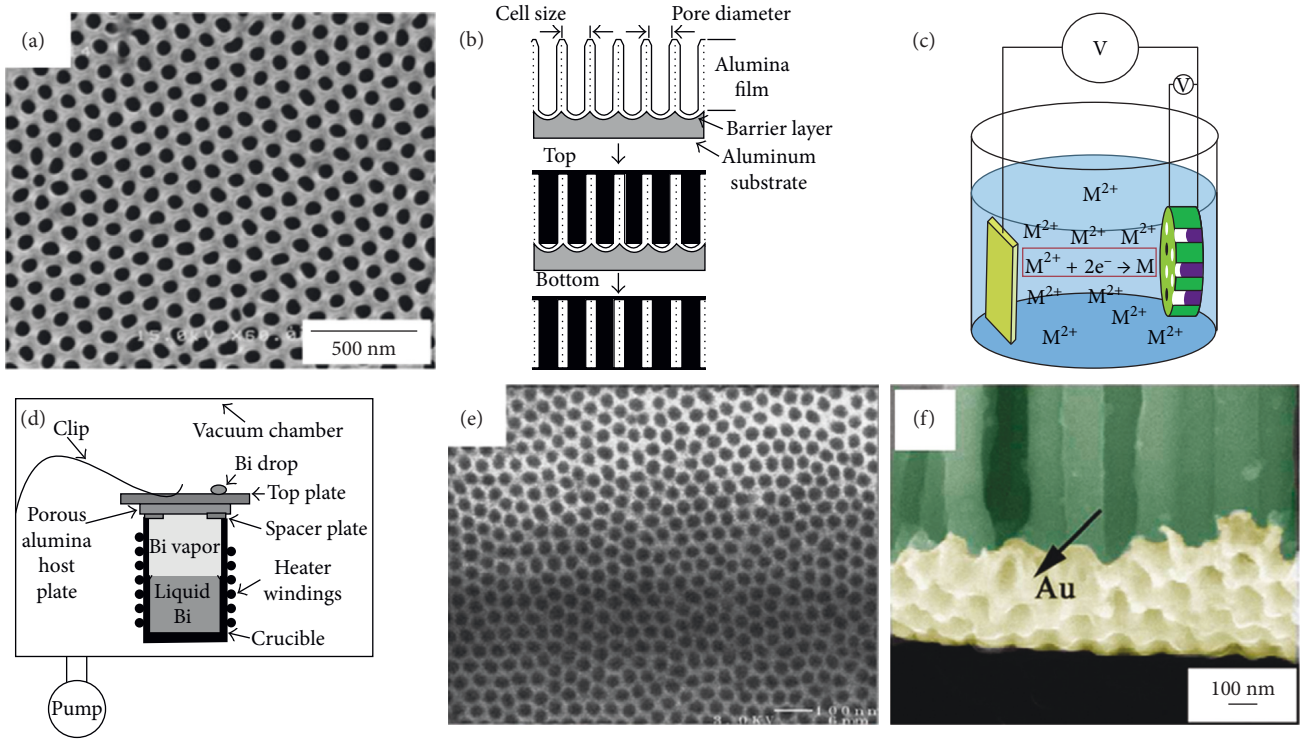

Figure 3: (a) Scanning electron microscope (SEM) image of an anodized aluminium oxide (AAO) template. (b) Growth mechanism in the liquid-phase method with an AAO template. (c) Schematic illustration of the electrochemical deposition in the AAO pores to fabricate nanowires. (d) Schematic diagram of the vacuum chamber, including a crucible for growing the nanowires by vapor-phase deposition. (e) SEM image of Bi nanowires in an AAO template. (f) SEM image of Bi nanotubes prepared by electrochemical deposition in an AAO template. Reprinted with permission from [75] Cambridge University Press, [76] American Institute of Physics, and [77] American Physical Society.

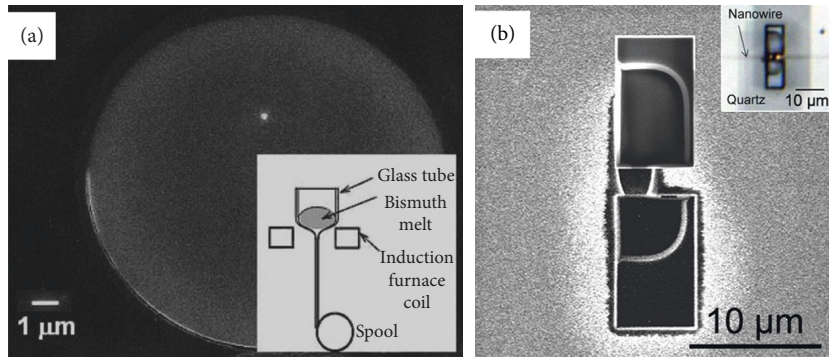

Figure 4: (a) Cross-sectional SEM image of a Bi nanowire grown by (a) the Ulitovsky method (the inset diagram outlines the growth mechanism) [70] and (b) pressurized injection in a quartz template [80]. Rreprinted with permission from [69] American Physical Society and [79] © 2012 Masayuki et al., originally published in *Nanoscale Research Letters*, vol. 7, p. 505, 2012, doi: 10.1186/1556-276X-7-505, under CC by 2.0 license.

Ulitovsky method [68, 70], negligible contamination, and smaller optical loss of quartz in comparison with borosilicate glasses, the hole and accordingly the diameter of the nanowires (~100 nm) seems yet too large to achieve optimal performance in some applications such as those requiring optical resonances in the UV region [7].

3.2. Stress-Induced Method. In several composite films with immiscible components such as Bi-CrN [71], Bi-Al [81], and Bi-Co [82], the compressive stresses could force the Bi to squeeze out and form nanowires. Utilizing the difference between the thermal expansion coefficients of the Bi thin film and a substrate or cap layer [27, 83], the compressive stresses can be also introduced by heating close to the melting temperature of Bi, and accordingly the Bi nanowires grow to release the induced thermal stress (Figures 5 (a) and 5(b)). Such stress-induced method is named as OFF-ON (on film formation of nanowires) and has been extended to other systems [27, 84]. In this method, the

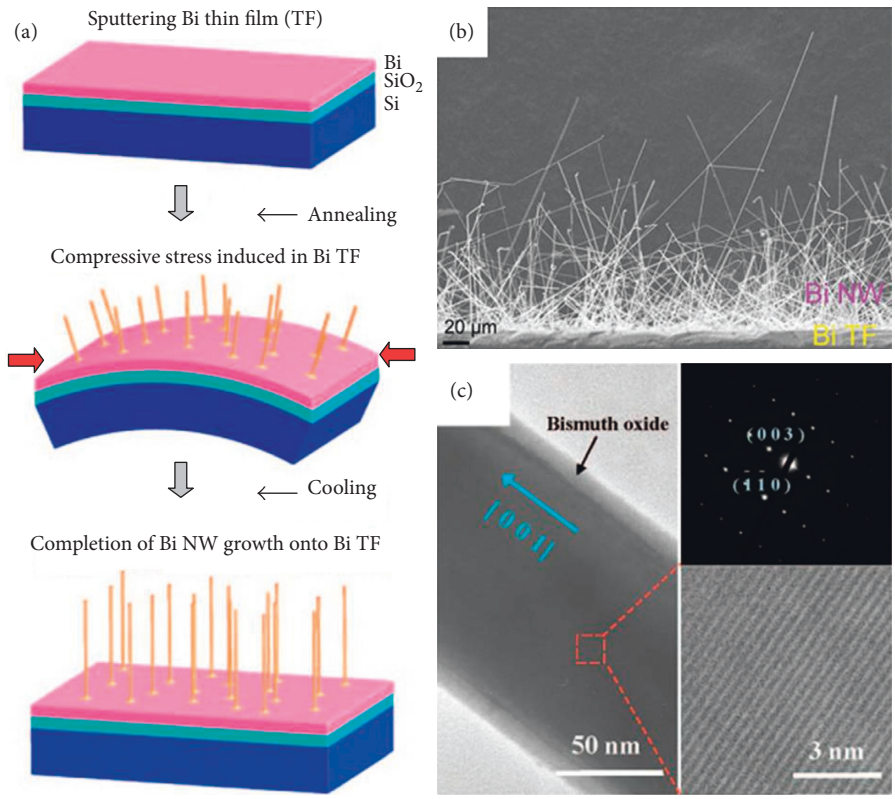

Figure 5: (a) Schematic representation of the growth mechanism by the OFF-ON method. (b) SEM image of the grown Bi nanowires. (c) Transmission electron microscope (TEM) image of a Bi nanowire and its electron diffraction patterns and crystal structure [27]. Reprinted with permission from American Chemical Society.

nanowire length and diameter can be controlled, respectively, via the heating time and the grain size of the Bi thin film deposited, for instance, on a thermal-oxidized silicon wafer (diameters between 21 nm and 10 μm and lengths up to several millimeters) [27]. The nanowires present a rather random orientation on the substrate (Figure 5(b)), but their growth occurs with a major crystal orientation in the [100] direction (Figure 5(c)) [27]. As a template-free method, the obtained Bi nanowires are free of the contaminations from chemical solutions or templates. However, because such nanowires do not present any initial passivation layer over the surface, further oxidation could generate during the fabrication or characterization (e.g., Raman spectra measurement) [85, 86].

3.3. PVD Growth of Bi Nanowires. Recently, it was found that vapor-deposition of Bi in specific conditions enables the spontaneous growth of nanowires [38, 41, 87, 88]. The attraction toward the PVD growth of Bi nanowires is that it can more readily produce structures that have a high degree of perfection in terms of crystallinity and regularity of the surface [38, 41, 87, 88]. Moreover, this method allows achieving a scalable nanowire growth and particularly dense wire populations [41, 87]. A higher conversion yield (>70%) from the deposited material to nanowires is also possible compared with the few-percent conversion of the stress-induced method [39]. Table 1 gathers selected cases for the PVD-growth of Bi nanowires reported in recent years: the processing temperature is relatively low (RT-200°C), the wire diameter ranges from 50 nm to 1 μm, and the length could reach tens of microns. Although the growth mechanisms of the Bi nanowires are under intense debate [86], generally, they can be catalogued into two main kinds: tip growth and root growth [39, 86].

In most reports about the PVD growth of Bi nanowires, the tip-growth mode (as shown in Figure 6(a)) seems to dominate. The growth starts from specific nuclei that form on the (initially) deposited bismuth film (step i to step ii), which might be screw dislocations, whiskers, hillocks, and grains [38, 86, 88]. These nuclei are related with lattice planes for preferential growth, which could be (110), (111), or (012) facet [41, 86]. Afterwards, the incoming Bi atoms would continuously migrate to preferential facets (step ii to step iii), resulting in the nanowire formation along the preferential direction with the growth front at its tip as shown in Figure 6(b). The wires with [110] or [012] orientation was found in the tip-growth cases [38, 40, 42]. The deposition rate has to be relatively low to provide a long adatom diffusion time [42], and accordingly, the growth of the nanowires is slow (typically it takes ten minutes to grow a ~10 μm nanowire) [38, 86, 88]. Moreover, high-rate diffusion of Bi adatoms is necessary for their long-distance motion to the tip. Therefore, sufficient kinetic energy and substrate heating are usually required [88]. Of course, if the deposition rate is low enough, the 1D growth is still

Table 1: The direct growth of Bi nanowires by PVD methods.

Growth technique	Temperature (°C)	Deposition rate (nm/s)	Length (μm)	Diameter (nm)	Growth time (min)	Substrate
Tip growth						
RF sputtering	200	0.67	~10	140	10	Si (111) [88]
RF sputtering	200	0.7	10s	100~300	10	Transition metal films (Fe, Ni, and Co) and W, Pt, and Au on oxidized Si, Si (111), oxidized Si (100), and fused quartz [86]
RF sputtering and thermal evaporation	110~140	0.04~0.12	16 ± 1	500	70~210	Glass, Si (100), Si (111), and GaAs (100) [38]
RF sputtering	120	0.03~0.09	3~16	80~120	18.5~55	Si (111) [40]
RF sputtering	RT~200	0.044~0.341	3~40	80~400	40	Si and glass [41]
Root growth						
RF sputtering	120~160	4	10~50	171~1800	4	Glass [87]
RF sputtering	0~75	0.1~0.2	0.5~30	60~200	4.2~8.3	Porous vanadium film [39]

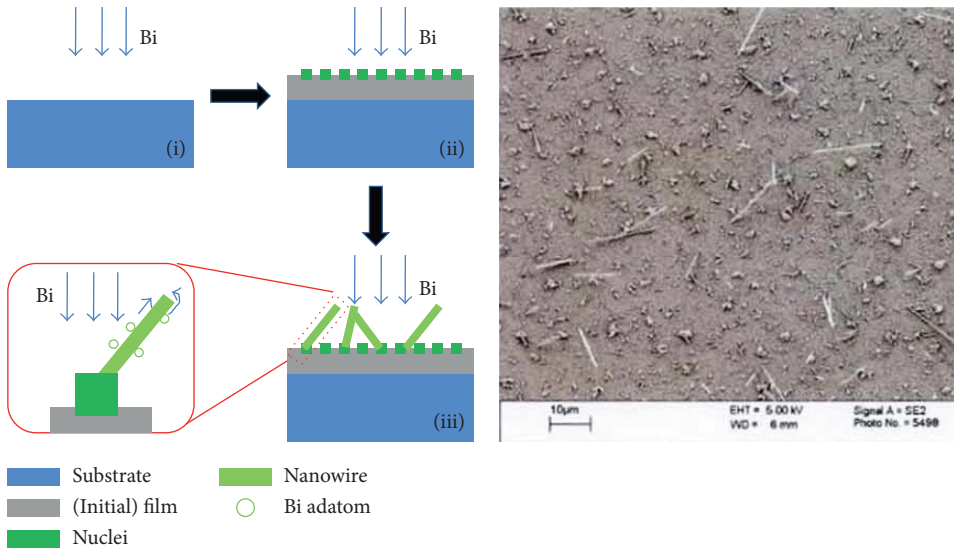

Figure 6: (a) Schematic representation of the tip-growth mode. (b) SEM image of Bi nanowires following the tip-growth mode. Reprinted from © Steven Antony Stanley, "The growth, structure and electrical properties of PVD deposited thin films and nanostructures of bismuth and antimony [D]" (2009), under CC by 2.5 license.

possible at room temperature and even by deposition with thermal evaporation, despite the formed nanowires being rather short (i.e., the growth becomes very slow) [42]. Additionally, it is noteworthy that, in the tip-growth mode, as the deposition time is long enough, the nanowire growth stops when a certain nanowire length is reached because the diffusing atoms are too far away from the tip to reach it [86].

For the root-growth mode, the extrusion of Bi on porous vanadium is a representative example [39]. In this case, first, Bi is deposited on a columnar vanadium thin film into which it infiltrates (Figures 7(a) and 7(b)). Due to the low wetting of vanadium with Bi, Bi exodiffuses from the pores and agglomerates at the surface to form a nucleation center (Figure 7(c)). Later in the deposition, incoming Bi atoms diffuse toward the nucleation centers where nanowires grow along the [012] direction with the growth front at their root (Figure 7(d)) [39]. Figure 7(e) shows the cross-sectional transmission electron microscopy (TEM) image of a Bi nanowire on the vanadium film as well as the energy dispersive X-ray spectra (EDX) mapping near the nanowire-vanadium film interface. Probably because a time-consuming adatom surface diffusion to the tip is not needed in the root-growth mode, the wire-growth speed (typically, it takes just few minutes to grow to ~10 μm length) seems faster than the tip growth [39]. Such a mechanism may also take effect in the quick nanowire growth along the [110] direction during the high-rate deposition of Bi on glass [87], where the initially deposited Bi atoms form nanoparticles which might play a role very similar to that of the agglomerated domains on columnar vanadium thin film [39]. However, without the excess surface energy provided by a columnar morphology to enable the highly directional and ballistic motion of the incoming Bi, a high deposition rate is needed to supply plenitudinous Bi timely for (fast) root growth [87].

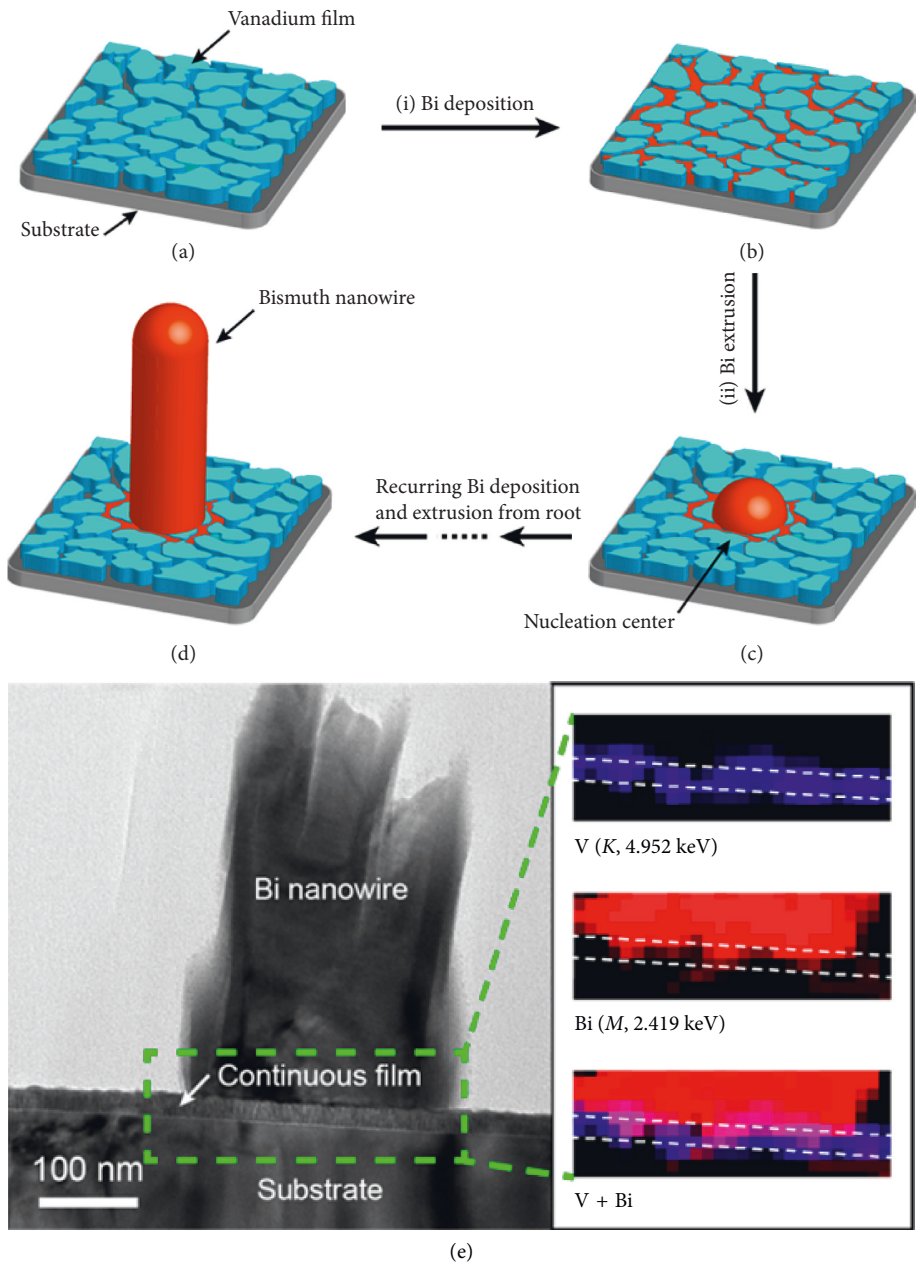

FIGURE 7: (a–d) Simplified representation of the growth of a Bi nanowire on a vanadium film following the root-growth mode. (e) TEM image of a Bi nanowire on the substrate. The energy dispersive X-ray (EDX) mapping of the distribution of the different species is also shown [39]. Reprinted with permission from the American Chemical Society.

3.4. Chemical Synthesis of Nanobismuth. Several chemical synthesis strategies, including the hydrothermal process, solution-phase process, thermolysis method, bottom-up assembly, polymer-assisted polyol process, solvothermal growth, aqueous chemical route, and electrochemical deposition, are widely applied for preparing a wide variety of Bi nanostructures such as nanobelts, nanosheets, nanospheres, nanowires, and nanotubes [26, 44–46, 48, 50, 54–56, 58, 72, 73, 89–91]. Although the starting materials and the synthesis conditions, as well as the growth mechanisms, in these reports show markedly different features, the growth processes can be divided into three steps as shown in Figure 8(a): (1) the reduction of Bi precursors into Bi. In this step, several materials, such as $NaBiO_3$, Bi $[N(SiMe_3)_2]_3$, $Bi(NO_3)_3$, biacetate, bicitrate, and $BiCl_3$, can serve as the Bi source to be reduced; (2) the agglomeration of Bi into nuclei; and (3) Bi nanostructure growth from these nuclei in a liquid phase including a dispersant or surfactant (such as polyethylene glycol, poly(1-vinylpyrrolidone)-graft-(1-hexa, decene) cetyltrimethylammonium bromide, sodium oleate, polyvinylpyrrolidone, and oleylamine). Such products, which are usually but not always needed, provide a spatially constrained reaction environment. Note that an intrinsic anisotropy, such as different surface energies at different lattice facets, or an externally produced anisotropy, allows synthesizing final products with a nonisotropic shape. Therefore,

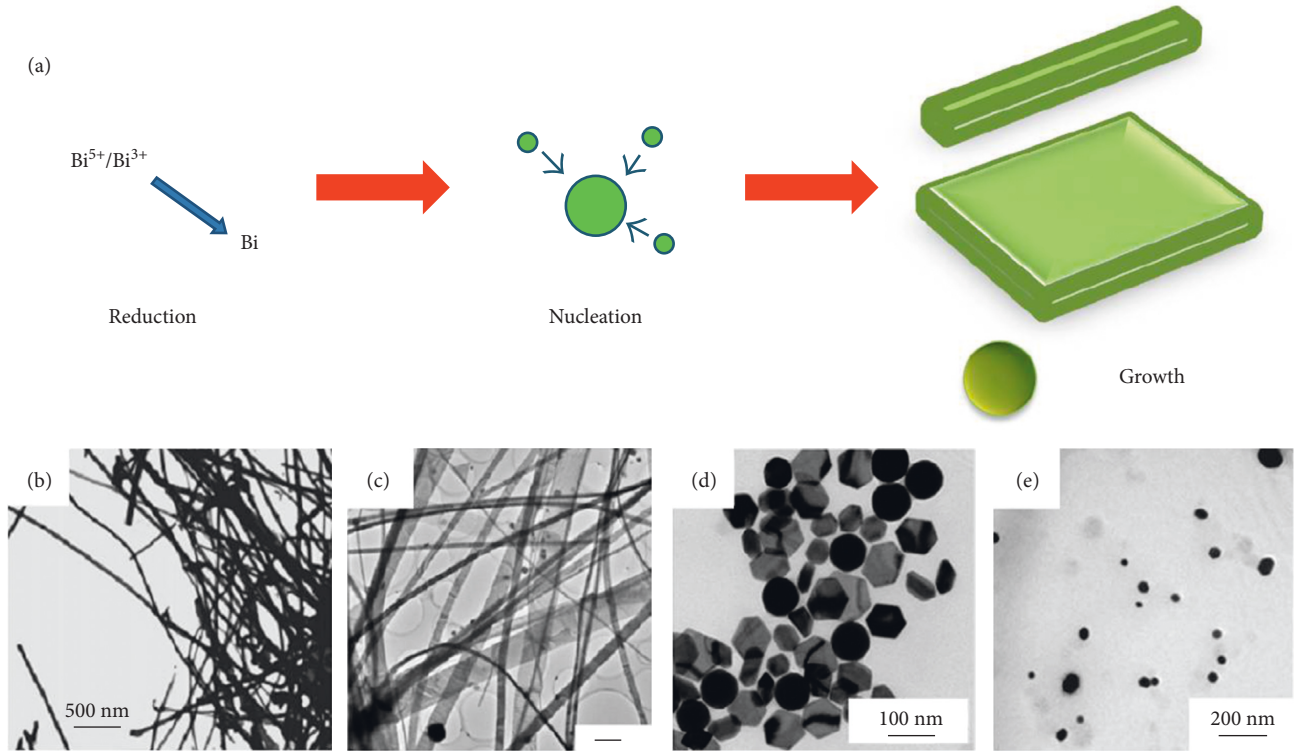

FIGURE 8: (a) Schematic representation of the Bi nanostructure growth by solution synthesis. TEM image of (b) Bi nanowires [44], (c) Bi nanobelts [73], (d) Bi nanoplates [47], and (e) Bi nanoparticles [52] prepared via solution synthesis, and the scale bar in (c) is 100 nm. Reprinted with permission from the American Institute of Physics and American Chemical Society.

upon rational tuning of the synthetic parameters and reaction conditions, the size and shape of the Bi nanostructures can be well controlled (Figures 8(b)–8(e)), and different lattice orientations were observed. However, due to the potential contamination from the solvent, dispersant, or surfactant, the crystalline quality of the products is poorer than that obtained following the stress-induced or PVD growth methods.

3.5. Laser-Assisted Processing. Bismuth nanostructures can also be prepared by laser-assisted methods. Basically, using these methods, a laser beam is used to vaporize or ablate Bi from a target, and then the products are collected on a substrate or directly dispersed in a liquid as shown in Figures 9(a)–9(c). The process can be carried out in a vacuum chamber, as done for the pulsed laser deposition (PLD) of Bi thin films or Bi nanoparticles embedded in an Al_2O_3 matrix [35, 63]. It can also be carried out using Ar gas as the matter-transport media, as done for the preparation of Bi nanoparticles by pulsed laser ablation (PLA) [37]. Using the Bi target containing 1% of Au catalyst, and using an Ar/H_2 mixed gas as matter-transport flow, a Bi nanorod growth was found to occur along the [012] direction [43]. Bi nanoparticle growth was also reported by ablation in liquids such as lubricant oils, where the obtained colloidal solution could be very suitable for tribological applications [51]. The crystalline quality of the products prepared by laser-assisted methods is moderate (Figures 9(d) and 9(e)), but the shortcoming is their relative broad size-distribution and/or poor shape-control as shown in Figures 9(f) and 9(g) [51].

3.6. Other Methods. Other methods to prepare Bi nanostructures include EBL [74], EM [61], MBE [62, 92], thermal decomposition [50], electron-beam irradiation [53], hydrothermal etching [46], and plasma force [57]. The EBL method is suitable for well defining the position, the shape, and the dimension of the nanostructures but expensive and limited to small area samples. The EM method can yield [110]-oriented Bi nanowires, with a diameter that can be reduced by a precisely controlled current though the wire. Bi atoms deposited on graphite surface by MBE showed 1D growth driven by anisotropic corner crossing. Bi nanoparticles were also obtained by thermal decomposition of Bi granules or prepared in situ under electron-beam irradiation to sodium bismuthate. Bi nanospheres on a Si surface were prepared by using low energy plasma focusing, or hydrofluoric acid-free hydrothermal etching.

4. Optical and Plasmonic Properties of Nanobismuth

4.1. UV-Vis-Near-IR Spectral Region

4.1.1. Theory: Interband Plasmonic Resonances in Bi Nanostructures. As explained in Section 2.2 in the UV-Vis-near-IR spectral region, the real part of the dielectric function of bulk Bi takes negative values ($\varepsilon_1 < 0$). Assuming that the dielectric function of Bi nanostructures is comparable to that of bulk Bi, this makes possible a plasmonic behavior for such nanostructures in the UV-Vis-near-IR. For a spherical

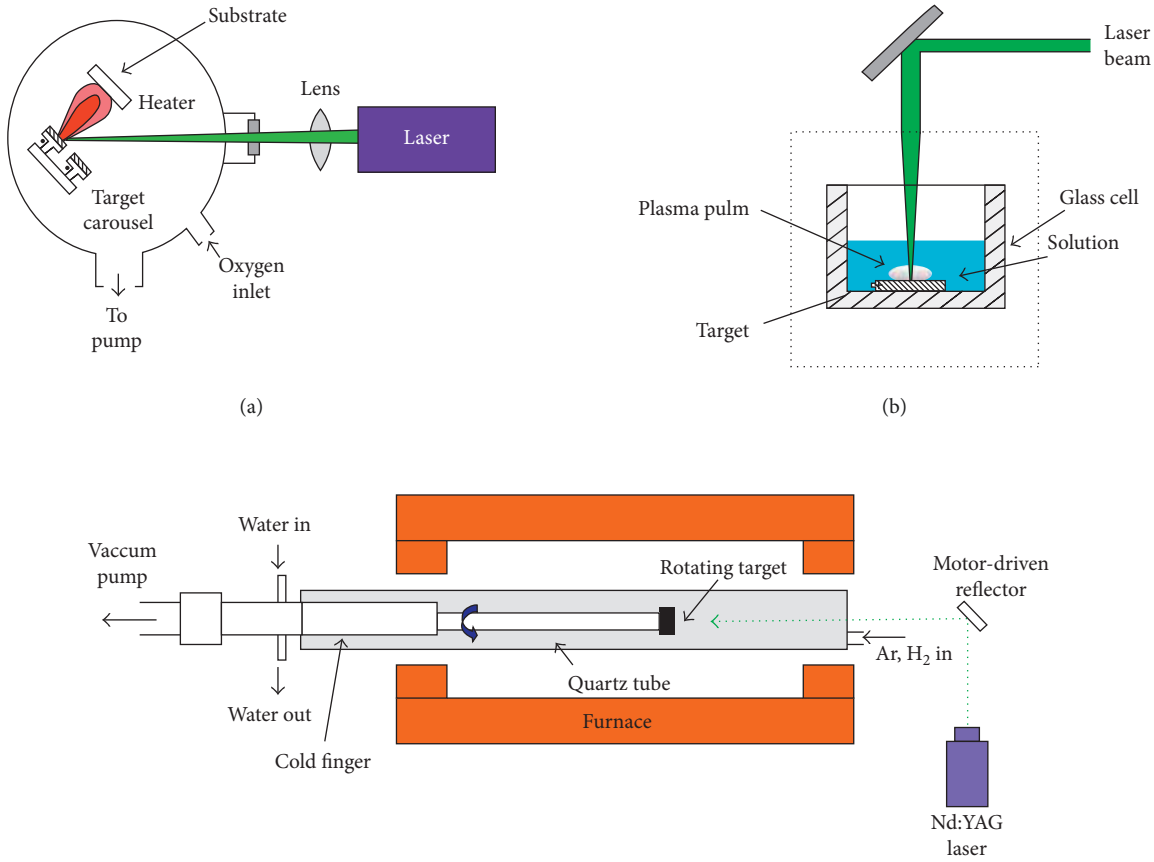

Figure 9: Continued.

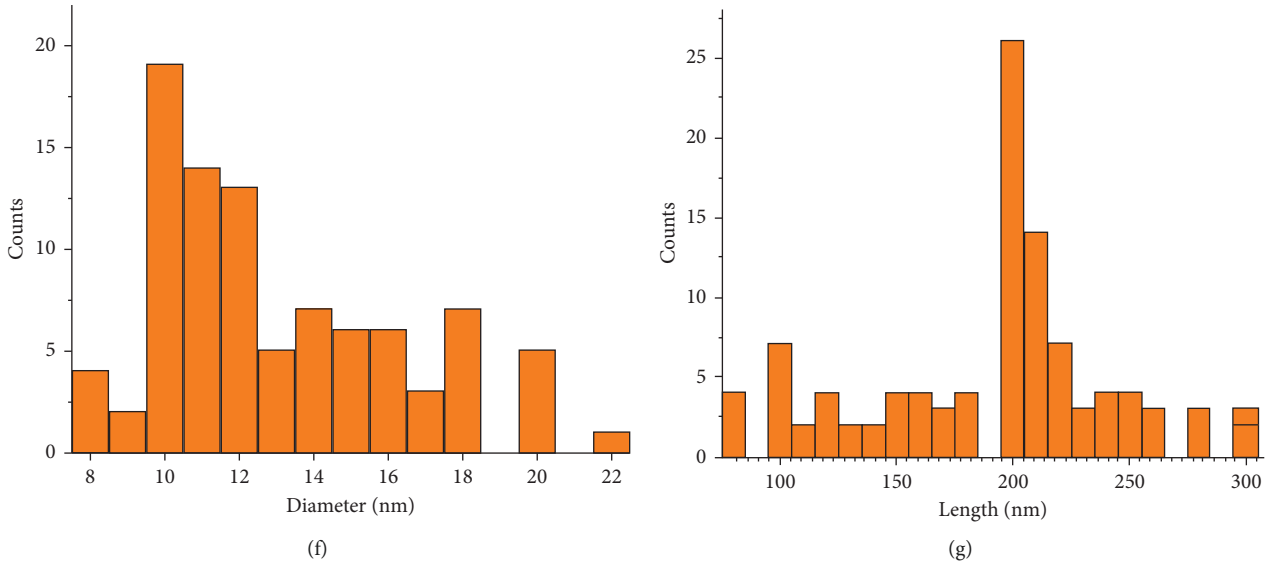

FIGURE 9: Schematic representation of laser-assisted fabrication of Bi nanostructures (a) in vacuum, (b) with matter-transport gas, and (c) in a liquid. (d) TEM image of a Bi nanorod produced by laser ablation and (e) its corresponding lattice fringes. (f) Diameter and (g) length distribution of the Bi nanorods [43]. Reprinted with permission from Reppert, Jason, "Laser-assisted synthesis and optical properties of bismuth nanorods" (2007), All Theses, 188.

nanostructure much smaller than the wavelength of the incident light and with e2 weakly dependent on E, quasi-static plasmonic resonance with a dipolar character occurs at the photon energy where $\varepsilon_1(E) = -2\varepsilon_m$, with ε_m being the real-valued dielectric function of the surrounding medium. This relation, also known as the Fröhlich condition, is fulfilled in the near UV for a Bi nanosphere in the usual embedding media such as SiO_2 or Al_2O_3 and can be approached in the visible region upon increasing ε_m [63]. For nonspherical Bi nanostructures, several quasi-static resonances are expected at different photon energies depending on the polarization of the incident light and on the nanostructure shape. For instance, in the case of spheroidal nanostructures, the Fröhlich condition becomes $\varepsilon_1(E) = (1 - 1/L_u)\varepsilon_m$, where L_u is the shape-dependent depolarization factor of the nanostructure along the direction u (along the spheroidal revolution axis or perpendicular to it). According to this relation, Bi nanospheroids can display two dipolar resonances: one for light polarized along the revolution axis (longitudinal resonance), and one for light polarized perpendicular to it (transverse resonance). Upon decreasing (increasing) the height-to-diameter ratio (or aspect ratio) of the spheroid, the transverse resonance shifts toward smaller (higher) photon energies and the longitudinal resonance toward higher (smaller) photon energies. This makes possible to bring one of the resonances deeper in the UV region than that of a Bi nanosphere and to drive the other across the visible toward the near-IR. This behaviour is thus comparable to that of localized plasmon resonances in noble metal (Ag and Au) nanostructures, however with a different origin. Instead of involving a collective oscillation of free carriers, they stand on the excitation of interband transitions that make the ε_1 of Bi turn negative in the UV-Vis-near-IR regions. Therefore, the term of "interband plasmonic" resonances has been proposed [35].

With the aim of addressing more quantitatively the features of such resonances than with the simplified picture of the quasi-static limit, several works have reported the use of analytical or numerical methods to compute the optical response of Bi nanostructures with sizes smaller or comparable with the wavelength of the incident light. Finite element method (FEM) [7], Mie [35, 54], and finite difference time domain (FDTD) [93] calculations have been used to simulate the optical cross sections of Bi nanospheres and their near-field enhancement for diameters up to a few hundreds of nm. The modified long wavelength approximation (MLWA) has been used to simulate the transverse optical cross sections of flattened Bi nanospheroids with diameter up to a few hundreds of nm [63]. FDTD calculations have been done to predict the transverse and longitudinal optical cross sections of Bi nanorods with lengths up to a few hundreds of nm and their near-field enhancement [64]. Maxwell's equations solving with the volume integral equation FFT method have been used to compute the optical extinction cross section of Bi nanospheres and nanoprisms and their near-field enhancement [94].

From these works, several predictions can be underlined:

(i) Upon increasing the diameter of a Bi nanosphere from a few nm to a few hundreds of nm, its extinction spectrum passes from being dominated by a single dipolar resonance that shifts from the UV to the visible region, to becoming a superposition of multiple order resonances spanning over the far UV-visible-near-IR region and showing no clear maximum in the visible [7, 93], as exemplified in Figure 10(a).

(ii) The dipolar resonance dominates the extinction spectrum of a Bi nanosphere while its diameter is lower than 100 nm. In these conditions, the resonance peaks in the UV or violet region (for a usual ε_m), where the extinction efficiency reaches values near 5 with a marked contribution of absorption

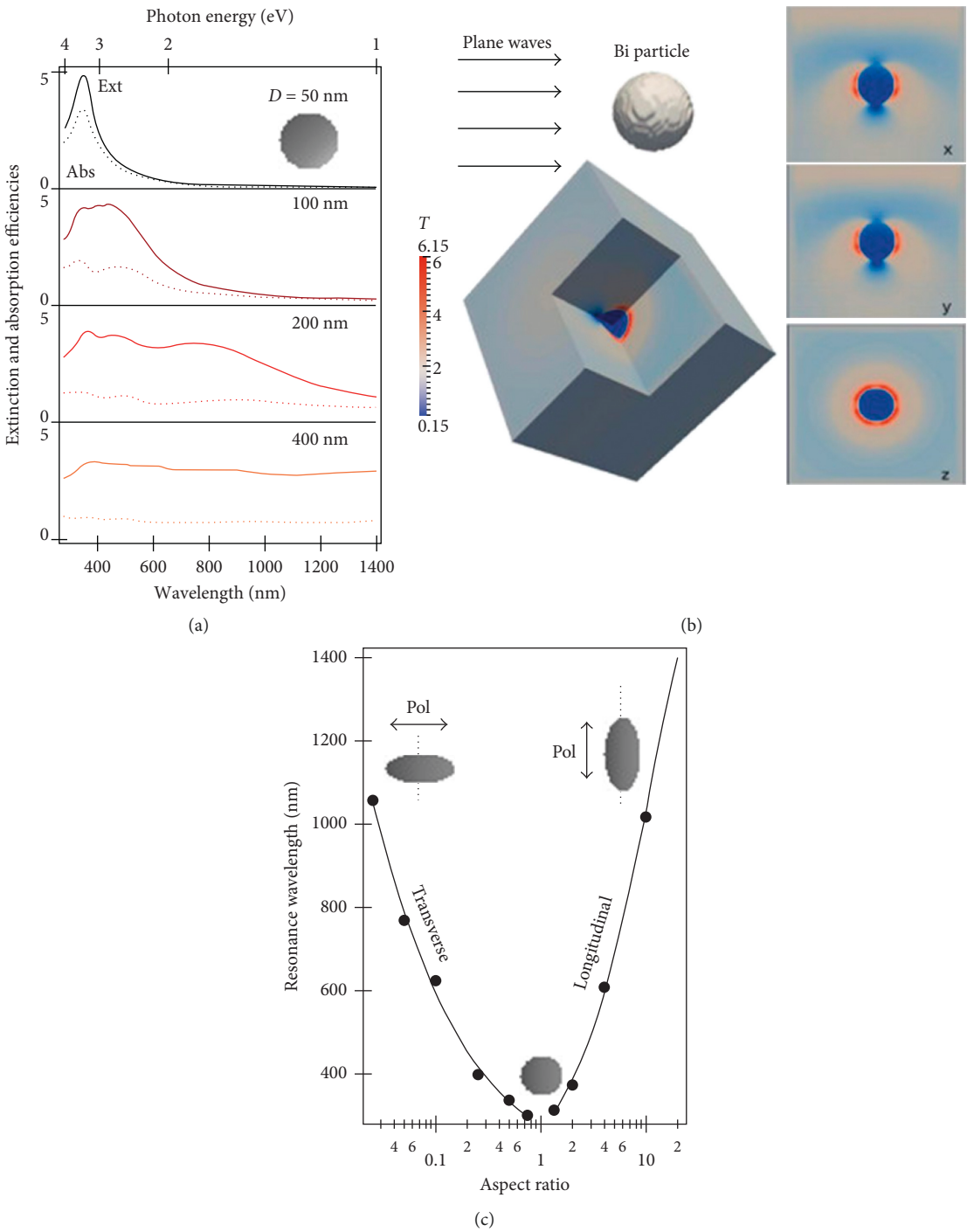

FIGURE 10: (a) Simulated extinction and absorption efficiency spectra of spherical Bi nanospheres of different diameter D, in water. Simulations have been done using the Mie theory and the dielectric function of Bi given in Figure 1. (b) Simulated near-field intensity (reprinted with permission from [105] © 2015, American Chemical Society). (c) Simulated resonant wavelengths of Bi nanospheroids in water, as a function of their aspect ratio. Simulations have been done using the Gans theory and the dielectric function of Bi given in Figure 1. For an aspect ratio <1 (>1), the transverse (longitudinal) resonance occurs in the UV-to-near-IR regions.

(Figure 10(a)). Such value is comparable with those found in the visible region for several metals and higher than those of Ag and Au nanostructures in the UV region [7, 93].

(iii) For a Bi nanosphere of any diameter, the dipolar and higher order resonances have a small quality factor (i.e., a broad spectral width) and induce a very small near-field enhancement (Figure 10(b)), due to the significant ε_2 values of Bi in the whole UV-Vis-near-IR region [63, 93].

(iv) The dipolar resonances of Bi nanorods or nanocylinders can be tuned across the UV to near-IR

region, with the corresponding extinction cross section remaining near 5, by controlling the nanostructure aspect ratio [63, 64] (Figure 10(c)).

From such results, it is evident that Bi nanostructures are interesting candidates for applications that require a strong absorption of light tunable in a broad spectral range from the UV to the near-IR region, such tuning being expected upon proper design. However, they are not suitable if high near-field enhancements or resonances with large quality factor are needed.

4.1.2. Experimental Observations. There is an increasing number of works reporting measurements of the UV-Vis-near-IR optical spectra of Bi nanostructures. The analysis of such reports provides valuable information for assessing the validity of the theoretical trends described above.

The earliest well-documented experimental work about the optical response of Bi nanostructures in the UV-Vis-near-IR was focused on solution processed Bi nanospheres diluted in water, with a diameter of $D < 10$ nm [95]. These nanospheres showed an absorption band in the mid-UV that was attributed to a plasmon resonance. More recent works reported the absorbance spectra of Bi nanospheres with a broader range of diameters: $D < 10$ nm, polydisperse Bi nanospheres with a low volume fraction in a glass matrix fabricated by melt quenching [96]; $D = 10$ nm, nearly monodisperse solution-processed Bi nanospheres diluted in hexane [97]; $10\,\text{nm} < D < 80\,\text{nm}$, solution-processed polydisperse Bi nanospheres diluted in ethanol [54]; $D = 100$ nm, vapor-deposited Bi nanospheres located with a low surface density at the mouths of an hexagonal-anodized TiO_2 honeycomb array [98]; and $50\,\text{nm} < D < 1\,\mu\text{m}$, nearly monodisperse surface-oxidized solution-processed Bi nanospheres as a dried powder [99].

A trend seems to emerge from these works, as seen in Figure 11(a). The absorbance spectrum of the nanostructures with $D \leq 10$ nm is dominated by a band peaking in the UV region. That of the polydisperse nanostructures with $10\,\text{nm} < D < 100\,\text{nm}$ consists of a broad band spanning in the visible region from blue to red photon energies. That of the biggest surface-oxidized Bi nanospheres spans over the whole visible region with no clear maximum. These trends are in qualitative agreement with the theoretical ones described above—point (i)—that predicted a shift of the dipolar interband plasmonic resonance from the UV to the visible region upon increasing D, followed by the onset of higher order resonances that yield a featureless extinction spectrum across the visible region.

Other works reported the UV-Vis-near-IR absorbance spectra of Bi nanostructures with nonspherical shapes, showing trends in agreement with theoretical predictions—point (iv) above. The absorbance spectra of coalesced Bi nanostructures in an Al_2O_3 medium was shown to include absorption bands characteristic of longitudinal and transverse resonances, the former being dominant and shifting from the near UV to the near-infrared as the nanostructure shape becomes more anisotropic, as seen in Figure 11(b) [63]. Pulsed laser-vaporized Bi nanorods in chloroform, with an aspect ratio of 20, displayed an absorption band in the near UV, attributed to a transverse plasmon resonance [100]. The spectral region of the measurement did not reach the photon energies where the longitudinal mode is expected for such aspect ratio.

Besides, the absorbance spectra of hybrid structures consisting of Bi nanostructures grown on dielectric nano- or microstructures (platelets, wires, and particles) have been reported in many works. In such structures, the Bi-related absorption peaks in the UV region for small Bi coverages and gradually extends to the whole UV region as the Bi coverage increases, as seen in Figure 11(c) [101–106]. This trend could be ascribed to the increasing size and degree of percolation of the Bi nanostructures as their coverage increases.

4.1.3. Quantum Confinement. Many of the trends observed experimentally for the UV-Vis-near-IR optical response of Bi nanostructures can be qualitatively accounted for by classical modeling. With such modeling, the dielectric function of the nanostructures is assumed to be the same as that of bulk Bi. However, several works have also proposed that quantum confinement effects in Bi nanostructures can modify their dielectric function compared with the bulk. Such modification could affect their optical properties in the UV-Vis-near-IR region.

When the size of a nanostructure becomes small enough (typically, smaller than the free charge carrier mean-free path in conductors, or exciton Bohr radius in excitonic semiconductors), its electronic structure (and thus its dielectric function) can depart from that of the corresponding bulk material and depend on the nanostructure size. In Bi nanostructures, it was proposed that such confinement effects can trigger a semimetal to semiconductor transition, which was reported first in thin films at a critical thickness near 30 nm [107]. The confined semiconducting Bi presents a bandgap that widens upon decreasing the nanostructure size. It was proposed that such bandgap widening can be strong enough so that the bandgap energy E_g reaches the UV-Vis-near-IR region ($E_g > 0.8$ eV) [108]. Such mechanism was used to interpret the blueshift in the optical absorption onset across the near-IR and visible regions for nanoparticles with truncated spheroidal shapes grown by sputtering deposition on transparent substrates, upon varying their size from a few tens of nm to a few nm [108]. In this work, the nanoparticle size was varied by tuning the amount of deposited Bi through the deposition time. By such method, it is worth noting that the shape and coverage of the nanoparticles vary together with their size. The same mechanism was also used to explain the near-IR absorption onset observed for $D = 3$ nm Bi nanospheres [109], and not for a bismuth powder. The existence of a bandgap widening due to confinement in Bi nanostructures was also discussed from the observation of their EELS spectra in the spectral region of their volume plasmons [52, 110, 111].

4.1.4. Partial Conclusion. Although a significant number of works have already reported the UV-Vis-near-IR optical

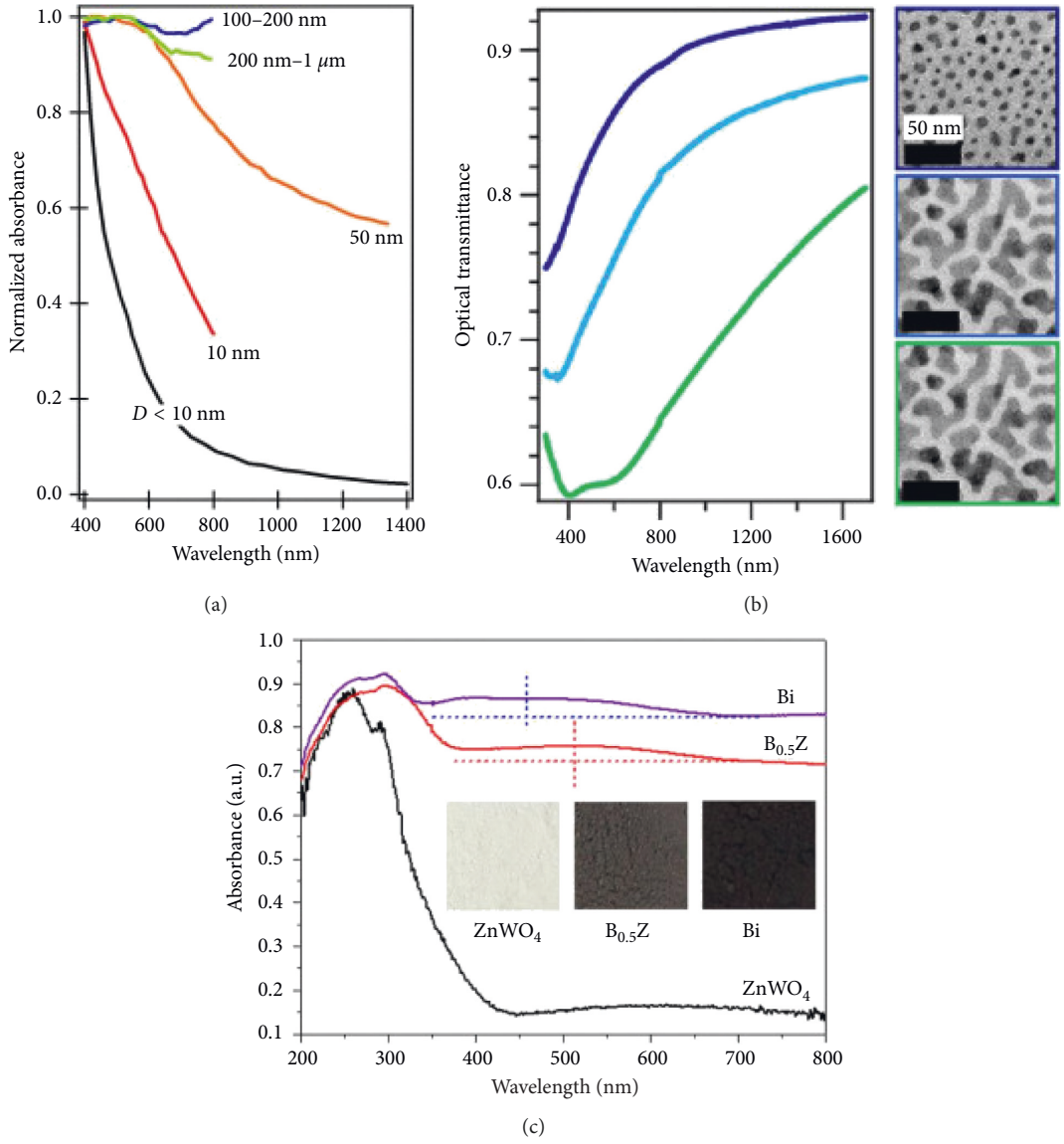

Figure 11: (a) Compilation of experimental absorbance spectra of Bi nanospheres (in liquids) with different diameters taken from the literature: <10 nm [96], 10 nm [97], 50 nm [54], 100–200 nm, and 200 nm–1 μm [99]. (b) Experimental transmittance spectra of assemblies of Bi nanostructures with different sizes and shapes (reprinted with permission from [63] © 2012, American Chemical Society). (c) Experimental absorbance spectra of a $ZnWO_4$ microsphere, a $ZnWO_4$ microsphere covered with Bi nanostructures, a Bi film (reprinted with permission from [103] © 2016, American Chemical Society).

properties of Bi nanostructures and main trends have been identified, there are still open questions to be answered. Especially, if the picture of "interband plasmonic" resonances predicted by classical models seems to support qualitatively many experimental results, the existence of quantum confinement effects impacting the UV-Vis-near-IR regions also has to be considered. In this context, it will be interesting to focus on Bi nanostructures with a better controlled size, morphology, and environment than in the already reported works, in order to get a better understanding of their UV-Vis-near-IR optical properties. Such a task seems feasible taking into account the broad range of available methods (described in Section 3) for synthesizing Bi nanostructures with controlled size and shape.

4.2. IR to THz Region

4.2.1. Quantum Confinement and Surface States. The optical properties of Bi nanostructures in the IR to THz region were studied in the early 2000s in order to probe quantum confinement effects in this spectral region. Especially, the optical absorbance spectra of Bi nanowires in the mid-IR appeared very different from that of thick Bi films. This difference was attributed to confinement-induced changes in

the mid-IR dielectric function of Bi [68, 112, 113]. In [68, 112], the characterization was performed on assemblies of nanowires that were initially grown inside the pores of nanoporous alumina templates. By such means, a small polydispersity was ensured for the nanowire dimensions. The authors used effective medium modeling to determine the dielectric function of the nanowires from the macroscopic measurement [68]. In [113], the measurements were done on a single nanowire deposited on a substrate, thus providing more direct information on its optical response.

Note that the dielectric function of a nanostructure reflects its effective response, which includes the contributions from its surface and volume. However, the electronic properties of these two regions can be significantly different in the case of Bi that may present metallic surface states, whereas the bulk has a semimetal character. Therefore, a more realistic description of the electronic and optical properties of a Bi nanostructure with high surface-to-volume ratio may require defining two dielectric functions: one for its surface and one for its volume. Considering such approach may become especially meaningful in the THz region for Bi nanostructures with a high surface-to-volume ratio, as suggested in [33] for ultrathin Bi films. In this work, a Drude analysis of THz transmittance spectra revealed a marked increase in the average free-carrier density (up to $10^{19}\,\mathrm{cm}^{-3}$) upon decreasing the film thickness below 10 nm. Such increase was attributed to the increasing contribution of metallic surface states to the film response. That points at the need of evaluating the role of surface states (that depend on the Bi facet exposed at the nanostructure surface) to interpret the optical response of Bi nanostructures with high surface-to-volume ratio, at least in the THz and IR regions, while their role in the UV-Vis regions seems less likely [109].

4.2.2. Infrared Plasmonics. More recently, there has been new interest in exploring the optical properties of Bi nanostructures in the IR to THz region, especially because of their potential for supporting plasmonic effects in the far-IR. In this spectral region, the ε_1 of Bi becomes negative (Figure 1) due to the contribution of free carriers. In this context, resonances were predicted and observed in the long-wave IR on Bi micrograting fabricated by evaporation of Bi on photoresist ridges designed by photolithography. The resonances were attributed to plasmonic modes [114, 115]. Far-IR resonances were also predicted theoretically in superlattices made of Bi layers and polaritonic materials [116], which could be fabricated by physical deposition techniques.

4.2.3. Mid- to Far-IR Dielectric Mie Resonances. Due to the high positive ε_1 (and thus high refractive index n) of bulk Bi in the mid- to far-IR, it can be expected that Bi nanostructures with dimensions of several hundreds of nm support dielectric Mie resonances in this region. Such resonances result from optical interference inside transparent or weakly absorbing nanostructures and thus, their wavelengths depend on the refractive index of these nanostructures. The higher the n, the shorter the resonance wavelength for a given nanostructure size. Since n reaches values near 10 for Bi in the mid- to far-IR, such resonances (that are based on optical interferences within the nanostructure) can be achieved for nanostructure sizes 10 times smaller than the wavelength of the incident light [19]. This is a quite remarkable fact, compared with usual dielectric nanostructures (based on oxides, Si, or Ge) that need to be designed with their size approaching the wavelength of the incident light to present a Mie resonance.

4.2.4. Partial Conclusions. The optical properties of Bi in the IR and THz regions are appealing for the development of nanostructures with resonant properties in these regions. However, this field remains to be explored, as there are quite few experimental demonstrations of such resonant effects.

5. Emerging Applications of Nanobismuth

Early, Bi nanostructures were considered as interesting candidates for applications to fields such as thermoelectricity or magnetism. More recently, the special optical and electronic properties of Bi have appealed to applications in new fields, such as photocatalysis, switchable plasmonic metamaterials, optoelectronics, or biology.

5.1. Photocatalysis. The most active research field focused on the applications of Bi nanostructures is certainly that of Bi-based photocatalysis, with hundreds of reports published in a few years. The interest in this field is based in particular on the low cost and low toxicity of Bi, which has been named "green metal" by some authors. Table 2 presents a selection of references where the photocatalytic properties of Bi-based materials were studied and specifies the chemical reactions that were considered.

The pioneering works on this topic [26, 54] demonstrated that Bi nanostructures can act as direct photocatalysts [26, 54, 117] (Figure 12(a)). In [26], solution-processed Bi nanoparticles diluted in water were used as the catalyst for nitric oxide (NO) removal. The solution in a dish was placed in a continuous flow reactor where air was introduced at a controlled flow rate and with a controlled concentration of NO at the sub-ppm level. UV light was shined with a filtered lamp on the catalyst, and the NO concentration was tracked by chemiluminescence. In these experimental conditions, NO removal ratios near 50% were reported for illumination times ranging from 10 to 300 minutes. In [54], solution-processed Bi nanospheres were used as the catalyst for the degradation of rhodamine B (RhB). The nanospheres were diluted in an aqueous RhB solution in a closed recipient. Visible light was shined on the solution with a lamp, and the RhB concentration was probed by monitoring the RhB absorption bands with a UV-visible spectrophotometer. In the reported experimental conditions, the presence of the Bi nanospheres was shown to enable an almost total RhB degradation after 10 hours, compared with only 10% degradation in a reference experiment without Bi nanospheres. To interpret such results, it is proposed that Bi nanostructures absorb efficiently the

Table 2: Bi-based photocatalysis on selected references.

Nanostructure type	Photocatalytic reaction	Spectral region	Reference
Bi nanospheres	RhB degradation (liquid)	Visible (380–830 nm)	[54]
Bi nanoparticles	NO degradation (liquid)	UV (280 nm)	[25]
Surface oxidized Bi nanospheres on TiO_2 nanotube array	—	—	[98]
Bi@Bi_2O_3 core-shell nanospheres	NO degradation	Visible (Xe lamp)	[99]
Bi films	NO degradation (air)	Visible (Xe lamp, 420 nm filter)	[101]
Bi_2O_3 nanospheres decorated with Bi nanoparticles	NO degradation (air)	Visible (halogen lamp, 420 nm filter)	[102]
$ZnWO_4$ nanospheres decorated with Bi nanoparticles	NO degradation (air)	Visible (halogen lamp, 420 nm filter)	[103]
Bi nanospheres on g-C_3N_4 nanosheets	NO degradation (air)	Visible	[105]
Bi nanoparticle-modified TiO_2 nanofibers	MO degradation (liquid)	UV (Xe lamp, 365 nm bandpass filter)	[106]
Bi nanoparticles w/graphene sheets	MO degradation (liquid)	Solar light	[116]
$(BiO)_2CO_3$ microstructures decorated with Bi nanoparticles	NO degradation (air)	Visible (halogen lamp, 420 nm filter)	[119]
N-doped $(BiO)_2CO_3$ microstructures decorated with Bi nanoparticles	NO degradation (air)	Visible (halogen lamp, 420 nm filter)	[120]
$(BiO)_2CO_3$ microstructures decorated with Bi nanoparticles	NO degradation (air)	Visible (halogen lamp, 420 nm filter)	[121]
$(BiO)_2CO_3$ microstructures decorated with Bi nanoparticles	NO degradation (air)	Visible (halogen lamp, 420 nm filter)	[122]
Bi nanoparticles on TiO_2 nanoparticles	RhB, phenol (liquid)	Visible (halogen lamp, 450 nm filter) and solar light	[123]
Bi nanoparticles on TiO_2 nanoparticles	Bromate (liquid)	Visible (Xe lamp, 400 nm filter)	[124]
$(BiO)_2CO_3$ platelets decorated with Bi nanoparticles	MB (liquid)	Visible (Hg lamp, 400 nm filter)	[125]

incident light and convert it into photocarriers that migrate to the nanostructure surface, where they can ease the formation of intermediates accelerating chemical reactions. The plasmonic resonances of Bi nanostructures certainly play a key role in this process because they enable a large optical absorption efficiency that is required for the efficient generation of photocarriers. Because such resonances can be tuned from the UV to the near-IR region by controlling the nanostructure size, shape, and environment, efficient photocarrier generation can be achieved in this spectral range. This has enabled Bi nanostructures to present a marked photocatalytic response under UV and also visible light. In this aspect, they are superior to other usual photocatalysts that operate mostly under UV light where their bandgap absorption occurs. One important point that was underlined [54] is that the potential of the photogenerated electrons (holes) must be low (high) enough so that they can efficiently trigger the chemical reaction of interest; this potential is defined by the photon energy of the incident photons. Furthermore, it was observed that a Bi_2O_3 shell at the surface of the nanostructures [99] can improve the photocarrier availability for chemical reactions if it is thin enough. The hybridization of Bi nanostructures with graphene [116] was also shown to improve such availability, the Bi-Bi_2O_3-graphene interface acting as a shuttle for photocarriers (Figure 12(b)).

Bi nanostructures have also been used as cocatalysts in hybrid materials, where they are in contact with larger semiconductor nanostructures. In most of the cases, NO removal was targeted, although the photocatalysis mechanism proposed to interpret the experimental results varied from one work to another (together with the nature and structure of the hybrid material), and some features highlighted in these reports can be mentioned here.

(i) Bi nanostructures allow enhanced photocatalytic capabilities in the visible region due to their strong achievable optical absorption efficiency [99, 118].

(ii) Bi nanostructures can scatter the incident light inside the semiconductor material, thus increasing the optical absorption efficiency and photocarrier generation in this material [102, 104–106, 119–122].

(iii) Depending on the electronic configuration of the hybrid (including potential of the photocarriers in the Bi nanostructure, location of the conduction, and valence band of the semiconductor), photocarriers, especially electrons, can flow from the Bi nanostructure to the semiconductor [94, 98, 103, 104, 119–123] or the opposite [105, 106, 124, 125]. Therefore, according to different reports, Bi nanostructures can act as an electron donor (the electrons being made available for reactions at the surface of the semiconductor, Figure 12(c)) or as electron acceptor (the electrons provided by the semiconductor reacting at their surface, Figure 12(d)).

Note that, although the reported works present detailed information about the structure of the studied materials, including crystallographic data of the Bi nanostructures (including high-resolution electron microscope and X-ray diffraction characterization), there has been no thorough investigation of the role of the exposed Bi crystal facets on their nanostructure catalytic properties. Because of the anisotropic electronic properties of Bi, this might be an interesting point to consider in further studies.

5.2. Switchable Plasmonic Metamaterials. Bi nanostructures have shown a potential as building blocks of switchable

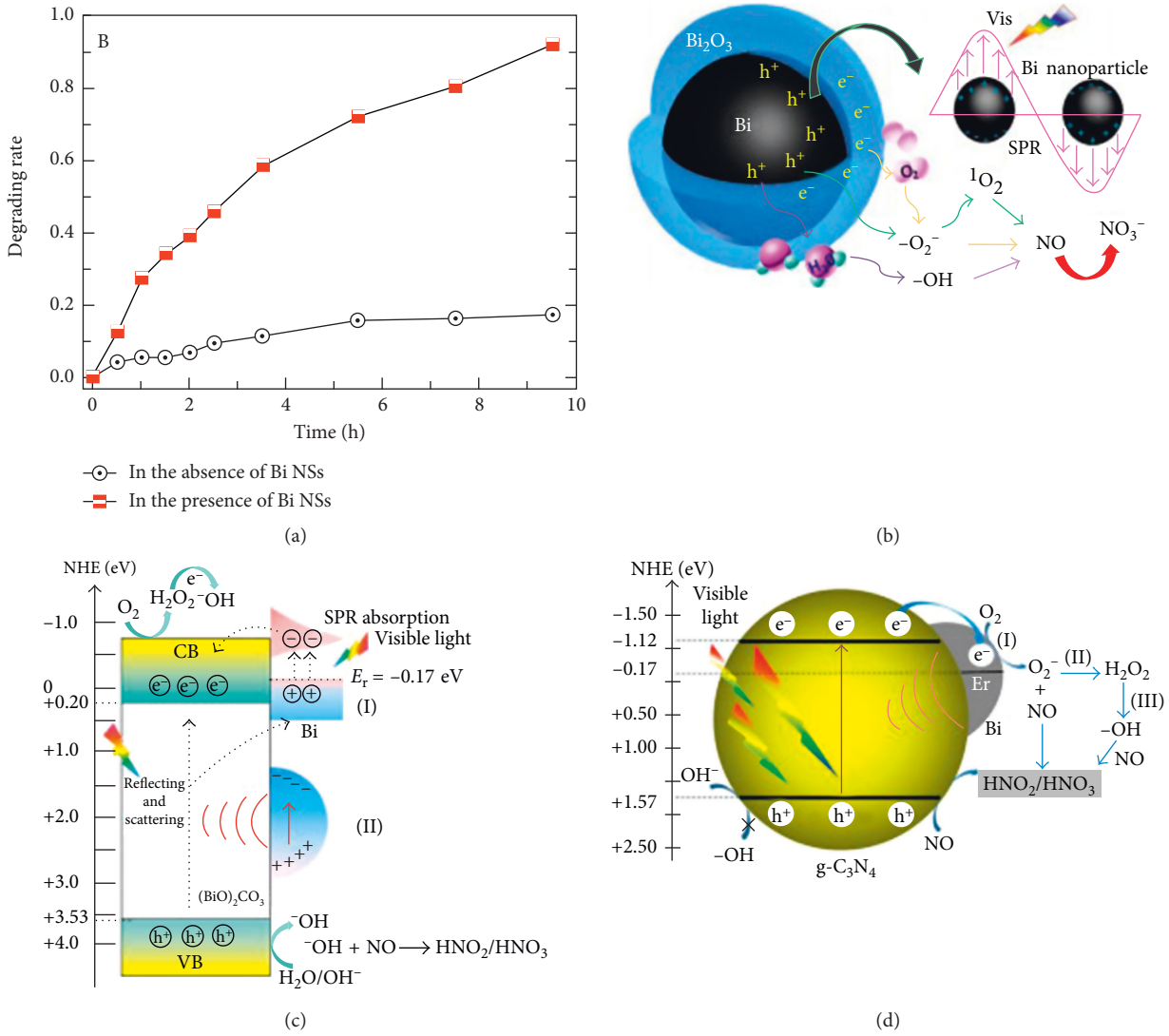

FIGURE 12: (a) Example of the photocatalytic effect of Bi nanospheres on the degradation rate of MO (reprinted from [54] © 2013, American Chemical Society). (b) Proposed mechanism for direct photocatalysis by a Bi nanosphere (reprinted with permission from [99] © 2017, American Chemical Society). (c) Proposed mechanism for the cocatalytic degradation of NO where Bi nanostructures act as an electron donor (reprinted with permission from [121] © 2014, American Chemical Society, under ACS AuthorChoice license). (d) Proposed mechanism for the cocatalytic degradation of NO where Bi nanostructures act as an electron acceptor (reprinted with permission from [105] © 2015, American Society of America).

plasmonic metamaterials. Switchable metamaterials show optical properties that are tunable dynamically upon external excitation, for instance by applying a voltage, changing the temperature, and irradiating with pulsed or continuous optical beams. During the last years, there has been a special interest in building switchable metamaterials from plasmonic nanostructures. In such materials, the plasmon resonances are tuned dynamically, either by changing the dielectric properties of the nanostructures (e.g., by carrier injection or phase transition) or of their environment (e.g., by phase transition of the surrounding medium and reorganization or reorientation of the nanostructures in a matrix). This way, the absorption by the metamaterial and its complex Fresnel coefficients can be tuned in real time in a selected spectral region, thus allowing a control of the intensity, polarization, and phase of light at specific photon energies. Switchable plasmonic metamaterials were developed using different component materials to cover a broad spectral range, mostly from the visible to the THz region. However, fewer solutions were available in the UV region.

Due to its capability to support plasmon resonances in the UV region and a solid-liquid phase transition that markedly modifies its dielectric function in this region, Bi has been used to fabricate nanomaterials with switchable absorption at UV photon energies [96]. In such materials, switching is enabled by the phase transition of Bi nanostructures embedded in a matrix. As the melting point of Bi is relatively low (270°C), the nanostructures can be molten and solidified many times reversibly while the matrix remains solid and acts as a mould that unables any change in the size and shape of the Bi

nanostructures. Only their dielectric function changes at the phase transition. Such change induces a shift in the nanostructures plasmon resonance, which enables measurable changes in the nanomaterial's absorbance at specific photon energies. Upon suitable tuning of the nanostructure size and shape, a dynamic switching of the nanomaterials absorbance can be expected not only in the UV region (nanospheres with $D < 100$ nm) but also across the visible region (larger nanospheres and nanorods) [7]. Yet, optimized metamaterials fully exploiting the switching potential of Bi nanostructures remain to be designed and fabricated. Furthermore, the switching potential of Bi nanostructures remains to be explored in the IR region. Also, note that another way of achieving optical switching with Bi nanostructures has recently been demonstrated: it has been demonstrated with light on ultrathin Bi films (also called "bismuthene") [126].

5.3. Other Applications. Several other applications have been proposed recently for Bi nanostructures. It has been proposed to use Bi thin films and nanorods as the active medium in photodetectors, based on their broadband absorption of light and excellent conduction properties involving surface states [127–129]. Despite their small near-field enhancement, they allow enhancing Raman signals [130]. They have been also used as low-toxicity contrast agents for medical tomography [131] and as nanoheaters for localized thermoradiotherapy [132].

6. Conclusions and Perspectives

Bismuth has motivated and attracted the interest of scientists during the past decades due to its thermoelectric, quantum confinement, and magnetoresistive properties. Only recently, Bi is becoming appealing for the applications involving its peculiar optical properties. Especially, an increasing interest is paid to subwavelength Bi nanostructures (or "nanobismuth") that show a potential for supporting optical resonances in a broad spectral region and are appealing for applications in nanophotonics, plasmonics, and even metamaterial engineering. In this article, we have presented a comprehensive review of the recent advances on this field: improved characterization of the optical response of bulk Bi, growth of Bi nanostructures, theoretical calculations, and experimental observations of their optical and plasmonic behaviour from the UV to the THz regions, emerging applications.

Bi nanostructures with a broad variety of sizes and shapes can be prepared with the following different existing fabrication methods:

(1) Template-based approaches, involving the liquid-phase injection, electrochemical, or vapor-phase deposition of Bi into AAO templates to form arrays of Bi nanowires or nanotubes; the Ulitovsky method or quartz template method for the growth of individual Bi nanowires.

(2) Template-free routes such as the stress-induced growth of nanowires and the direct PVD growth of Bi nanowire with tip- or root-driven modes.

(3) Chemical synthesis of Bi nanostructures with a broad variety of shapes from 0D to 3D.

(4) Laser-assisted fabrication of Bi nanoparticles.

Further developments are needed for improving the quality of nanobismuth, especially for achieving nanostructures while controlling their size, shape and organization, and developing techniques for device fabrication.

Classical electrodynamic simulations predict that Bi nanostructures are able to support so-called "interband plasmonic" resonances in the UV-Vis-near-IR range with dipolar or higher order modes, depending on the nanostructure size. Moreover, upon rational design (proper choice of the nanostructure size and shape), the strong absorption produced by such resonances is expected with a broad spectral tunability from the UV region to the near-IR region. However, due to the relatively low quality factor of such resonances, nanobismuth is not a good candidate for applications requiring, for instance high near-field enhancements. Yet, while the reported experimental data on the UV-Vis-near-IR optical response of Bi nanostructure show some qualitative agreement with classical electrodynamic calculations, the possible role of quantum effects has to be examined in detail. At such aim, the characterization of Bi nanostructures with better controlled size, shape, and environment is necessary. Classical electrodynamic simulations and recent experiments let foresee interesting optical properties of Bi nanostructures in the IR to THz regions, including Mie resonances and "traditional" plasmon resonances based on free-charge carriers. However, so far, there are quite few experimental demonstrations of resonant effects in Bi nanostructures in the IR to THz region, and more investigations on this issue are needed.

The optical resonances of nanobismuth—mostly in the UV-visible-near-IR—are triggering applications in an increasing number of fields. The "interband plasmonic" resonances enable the excitation of photogenerated electron-hole pairs, and thus, Bi itself becomes a quite attractive candidate for the photocatalysis with high energy conversion performance under both UV and visible illumination. Also, the enhanced light absorption and scattering, as well as the flexibility to play either as electron donor or electron acceptor depending on the needs, make Bi nanostructures a sound choice as cocatalyst in Bi/semiconductor hybrid systems. Besides its potential for photocatalysis, nanobismuth is a promising solution for switchable plasmonic metamaterials in the UV region and beyond, and the switching potential in the visible and IR region remain to be explored. Recent report on optical switching of ultrathin Bi films (also called "bismuthene") opens the possibility to further expand the potential of Bi nanostructures to switchable optoelectronic components. Note that, in most of the works that we have discussed, the influence of the crystal facets exposed at the surface of the Bi nanostructures on their optoelectronic functionalities has not been thoroughly evaluated. Because of the structural and electronic anisotropy of Bi and its facet-dependent surface states, the nature of the exposed facets might affect either the optical response of Bi nanostructures with a high surface-to-volume ratio (where surface states play

a significant role on the overall response) or their functionalities for applications in which surfaces are a key player (such as catalysis, surface-enhanced Raman spectroscopy, and charge transport).

In sum, the progresses on the fabrication of Bi nanostructures, the control and understanding of their optical response, and the emergence of alternative applications open new possibilities for nanobismuth beyond the already explored paths. More experimental observations are needed to explore the optical potential of nanobismuth over abroad spectral range (from the UV to the THz region). Further developments are also necessary to overcome the obstacles to achieve practical nanobismuth-based optical materials and devices.

Conflicts of Interest

The authors declare that they have no conflicts of interest.

Acknowledgments

This research was supported in part by the National Natural Science Foundation of China (nos. 61471164 and 11447120).

References

[1] W. L. Barnes, A. Dereux, and T. W. Ebbesen, "Surface plasmon subwavelength optics," *Nature*, vol. 424, no. 6950, pp. 824–830, 2003.

[2] D. Chen, J. Miao, Y. Tian, J. Zhang, and Q. Liu, "Field enhancement of tip with spiral nanostructure," *Plasmonics*, vol. 9, no. 6, pp. 1245–1249, 2014.

[3] G. Di Martino, S. Tappertzhofen, S. Hofmann, and J. Baumberg, "Nanoscale plasmon-enhanced spectroscopy in memristive switches," *Small Banner*, vol. 12, no. 10, pp. 1334–1341, 2016.

[4] P. D. Flammer, J. M. Banks, T. E. Furtak, C. G. Durfee, R. E. Hollingsworth, and R. T. Collins, "Hybrid plasmon/dielectric waveguide for integrated silicon-on-insulator optical elements," *Optics Express*, vol. 18, no. 20, pp. 21013–21023, 2010.

[5] R. W. Heeres, S. N. Dorenbos, B. Koene, G. S. Solomon, L. P. Kouwenhoven, and V. Zwiller, "On-chip single plasmon detection," *Nano letters*, vol. 10, no. 2, pp. 661–664, 2009.

[6] A. Melikyan, L. Alloatti, A. Muslija et al., "High-speed plasmonic phase modulators," *Nature Photonics*, vol. 8, no. 3, pp. 229–233, 2014.

[7] A. Cuadrado, J. Toudert, and R. Serna, "Polaritonic-to-plasmonic transition in optically resonant bismuth nanospheres for high-contrast switchable ultraviolet meta-filters," *IEEE Photonics Journal*, vol. 8, no. 3, pp. 1–11, 2016.

[8] T. M. Chien and W. H. Hung, "Observation of strong plasmonic heating in Au-Fe_2O_3 nanocomposite," *Materials Research Express*, vol. 1, no. 1, p. 015009, 2014.

[9] H. Chen, G. C. Schatz, and M. A. Ratner, "Experimental and theoretical studies of plasmon–molecule interactions," *Reports on Progress in Physics*, vol. 75, no. 9, p. 096402, 2012.

[10] S. T. Jones, R. W. Taylor, E. K. Abo Hamed et al., "Gold nanorods with sub-nanometer separation using cucurbit[*n*]uril for SERS applications," *Small*, vol. 10, no. 21, pp. 4298–4303, 2014.

[11] A. G. Brolo, "Plasmonics for future biosensors," *Nature Photonics*, vol. 6, no. 11, pp. 709–713, 2012.

[12] J. Yang, H. Giessen, and P. Lalanne, "Simple analytical expression for the peak-frequency shifts of plasmonic resonances for sensing," *Nano Letters*, vol. 15, no. 5, pp. 3439–3444, 2015.

[13] J. Yang, M. Perrin, and P. Lalanne, "Analytical formalism for the interaction of two-level quantum systems with metal nanoresonators," *Physical Review X*, vol. 5, no. 2, p. 021008, 2015.

[14] C. Langhammer, Z. Yuan, I. Zorić, and B. Kasemo, "Plasmonic properties of supported Pt and Pd nanostructures," *Nano Letters*, vol. 6, no. 4, pp. 833–838, 2006.

[15] I. Zorić, M. Zäch, B. Kasemo, and C. Langhammer, "Gold, platinum, and aluminum nanodisk plasmons: material independence, subradiance, and damping mechanisms," *ACS Nano*, vol. 5, no. 4, pp. 2535–2546, 2011.

[16] G. V. Naik, V. M. Shalaev, and A. Boltasseva, "Alternative plasmonic materials: beyond gold and silver," *Advanced Materials*, vol. 25, no. 24, pp. 3264–3294, 2013.

[17] N. Kinsey, M. Ferrera, G. V. Naik, V. E. Babicheva, V. M. Shalaev, and A. Boltasseva, "Experimental demonstration of titanium nitride plasmonic interconnects," *Optics Express*, vol. 22, no. 10, pp. 12238–12247, 2014.

[18] Z. Li, K. Yao, F. Xia, S. Shen, J. Tian, and Y. Liu, "Graphene plasmonic metasurfaces to steer infrared light," *Scientific Reports*, vol. 5, no. 1, p. 12423, 2015.

[19] J. Toudert and R. Serna, "Interband transitions in semimetals, semiconductors, and topological insulators: a new driving force for plasmonics and nanophotonics [Invited]," *Optical Materials Express*, vol. 7, no. 7, pp. 2299–2325, 2017.

[20] A. García-Etxarri, R. Gómez-Medina, L. S. Froufe-Pérez et al., "Strong magnetic response of submicron silicon particles in the infrared," *Optics Express*, vol. 19, no. 6, pp. 4815–4826, 2011.

[21] J. Heremans, C. M. Thrush, Y.-M. Lin et al., "Bismuth nanowire arrays: synthesis and galvanomagnetic properties," *Physical Review B*, vol. 61, no. 4, p. 2921, 2000.

[22] Z. Zhang, X. Sun, M. S. Dresselhaus, J. Y. Ying, and J. P. Heremans, "Magnetotransport investigations of ultrafine single-crystalline bismuth nanowire arrays," *Applied Physics Letters*, vol. 73, no. 11, pp. 1589–1591, 1998.

[23] Z. Zhang, X. Sun, M. S. Dresselhaus, J. Y. Ying, and J. Heremans, "Electronic transport properties of single-crystal bismuth nanowire arrays," *Physical Review B*, vol. 61, no. 7, p. 4850, 2000.

[24] F. Yang, K. Liu, K. Hong, D. H. Reich, P. C. Searson, and C. L. Chien, "Large magnetoresistance of electrodeposited single-crystal bismuth thin films," *Science*, vol. 284, no. 5418, pp. 1335–1337, 1999.

[25] F. Dong, T. Xiong, Y. Sun et al., "A semimetal bismuth element as a direct plasmonic photocatalyst," *Chemical Communications*, vol. 50, no. 72, pp. 10386–10389, 2014.

[26] J. Heremans and C. Thrush, "Thermoelectric power of bismuth nanowires," *Physical Review B*, vol. 59, no. 19, p. 12579, 1999.

[27] W. Shim, J. Ham, K. Lee, W. Y. Jeung, M. Johnson, and W. Lee, "On-film formation of Bi nanowires with extraordinary electron mobility," *Nano Letters*, vol. 9, no. 1, pp. 18–22, 2008.

[28] T. Huber, K. Celestine, and M. Graf, "Magnetoquantum oscillations and confinement effects in arrays of 270-nm-diameter bismuth nanowires," *Physical Review B*, vol. 67, no. 24, p. 245317, 2003.

[29] L. Li, J. G. Checkelsky, and Y. S. Hor, "Phase transitions of dirac electrons in bismuth," *Science*, vol. 321, no. 5888, pp. 547–550, 2008.

[30] C. F. Gallo, B. S. Chandrasekhar, and P. H. Sutter, "Transport properties of bismuth single crystals," *Journal of Applied Physics*, vol. 34, no. 1, pp. 144–152, 1963.

[31] Y. Fuseya, M. Ogata, and H. Fukuyama, "Transport properties and diamagnetism of dirac electrons in bismuth," *Journal of the Physical Society of Japan*, vol. 84, p. 012001, 2015.

[32] Y. Liu and R. E. Allen, "Electronic structure of the semimetals Bi and Sb," *Physical Review B*, vol. 52, no. 3, pp. 1566–1577, 1995.

[33] K. Yokota, J. Takeda, C. Dang et al., "Surface metallic states in ultrathin Bi (001) films studied with terahertz time-domain spectroscopy," *Applied Physics Letters*, vol. 100, p. 251605, 2012.

[34] R. Tediosi, N. P. Armitage, E. Giannini, and D. van der Marel, "Charge carrier interaction with a purely electronic collective mode: plasmarons and the infrared response of elemental bismuth," *Physical Review Letters*, vol. 99, no. 1, p. 016406, 2007.

[35] J. Toudert, R. Serna, I. Camps et al., "Unveiling the far infrared-to-ultraviolet optical properties of bismuth for applications in plasmonics and nanophotonics," *Journal of Physical Chemistry C*, vol. 121, no. 6, pp. 3511–3521, 2017.

[36] R. G. T. Rosa, C. A. Duarte, W. H. Schreiner et al., "Structural, morphological and optical properties of Bi NPs obtained by laser ablation and their selective detection of L-cysteine," *Colloids and Surfaces A: Physicochemical and Engineering Aspects*, vol. 457, pp. 368–373, 2014.

[37] S. Onari, M. Miura, and K. Matsuishi, "Raman spectroscopic studies on bismuth nanoparticles prepared by laser ablation technique," *Applied Surface Science*, vol. 197, pp. 615–618, 2002.

[38] S. A. Stanley, *The Growth, Structure and Electrical Properties of PVD Deposited thin Films and Nanostructures of Bismuth and Antimony*, Doctoral Dissertation, Steven Antony Stanley, Leicestershire, UK, 2009.

[39] M. Liu, J. Tao, C.-G. Nam, K. Kisslinger, L. Zhang, and D. Su, "Surface-energy induced formation of single crystalline bismuth nanowires over vanadium thin film at room temperature," *Nano Letters*, vol. 14, no. 10, pp. 5630–5635, 2014.

[40] A. J. Caruana, M. D. Cropper, and S. A. Stanley, "Spontaneous growth of bismuth nanowires on a sputter-deposited thin bismuth film," *Surface and Coatings Technology*, vol. 271, pp. 8–12, 2015.

[41] Y. Tian, C. F. Guo, S. Guo et al., "Bismuth nanowire growth under low deposition rate and its ohmic contact free of interface damage," *AIP Advances*, vol. 2, no. 1, p. 012112, 2012.

[42] Y. Tian, L. Jiang, X. Zhang, Y. Deng, and S. Deng, "Coexistence and competition of surface diffusion and geometric shielding in the growth of 1D bismuth nanostructures and their ohmic contact," *Materials Research Express*, vol. 1, no. 3, p. 035034, 2014.

[43] J. Reppert, R. Rao, M. Skove et al., "Laser-assisted synthesis and optical properties of bismuth nanorods," *Chemical Physics Letters*, vol. 442, no. 4–6, pp. 334–338, 2007.

[44] J. Wang, X. Wang, Q, Peng, and Y. Li, "Synthesis and characterization of bismuth single-crystalline nanowires and nanospheres," *Inorganic Chemistry*, vol. 43, no. 23, pp. 7552–7556, 2004.

[45] Y. Chen, R. Gong, W. Zhang, X. Xu, Y. Fan, and W. Liu, "Synthesis of single-crystalline bismuth nanobelts and nanosheets," *Materials Letters*, vol. 59, no. 8, pp. 909–911, 2005.

[46] H. Liu and Z. L. Wang, "Bismuth spheres grown in self-nested cavities in a silicon wafer," *Journal of the American Chemical Society*, vol. 127, no. 43, pp. 15322–15326, 2005.

[47] F. Wang, R. Tang, H. Yu, P. C. Gibbons, and W. E. Buhro, "Size-and shape-controlled synthesis of bismuth nanoparticles," *Chemistry of Materials*, vol. 20, no. 11, pp. 3656–3662, 2008.

[48] Y. Xu, Z. Ren, W. Ren, G. Cao, K. Deng, and Y. Zhong, "Magnetic-field-assisted solvothermal growth of single-crystalline bismuth nanowires," *Nanotechnology*, vol. 19, no. 11, p. 115602, 2008.

[49] P. Kumar, J. Singh, and A. C. Pandey, "Rational low temperature synthesis and structural investigations of ultrathin bismuth nanosheets," *RSC Advances*, vol. 3, no. 7, pp. 2313–2317, 2013.

[50] Y. Zhao, Z. Zhang, and H. Dang, "A simple way to prepare bismuth nanoparticles," *Materials Letters*, vol. 58, no. 5, pp. 790–793, 2004.

[51] M. Flores-Castañeda, E. Camps, M. Camacho-López, S. Muhl, E. García, and M. Figueroa, "Bismuth nanoparticles synthesized by laser ablation in lubricant oils for tribological tests," *Journal of Alloys and Compounds*, vol. 643, pp. S67–S70, 2015.

[52] Y. Wang, J. S. Kim, G. H. Kim, and K. S. Kim, "Quantum size effects in the volume plasmon excitation of bismuth nanoparticles investigated by electron energy loss spectroscopy," *Applied Physics Letters*, vol. 88, no. 14, p. 143106, 2006.

[53] S. Sepulveda-Guzman, N. Elizondo-Villarreal, D. Ferrer et al., "In situ formation of bismuth nanoparticles through electron-beam irradiation in a transmission electron microscope," *Nanotechnology*, vol. 18, no. 33, p. 335604, 2007.

[54] Z. Wang, C. Jiang, R. Huang, H. Peng, and X. Tang, "Investigation of optical and photocatalytic properties of bismuth nanospheres prepared by a facile thermolysis method," *Journal of Physical Chemistry C*, vol. 118, no. 2, pp. 1155–1160, 2013.

[55] J. Wu, H. Yang, H. Li, Z. Lu, X. Yu, and R. Chen, "Microwave synthesis of bismuth nanospheres using bismuth citrate as a precursor," *Journal of Alloys and Compounds*, vol. 498, no. 2, pp. L8–L11, 2010.

[56] G. Cheng, J. Wu, F. Xiao et al., "Synthesis of bismuth micro- and nanospheres by a simple refluxing method," *Materials Letters*, vol. 63, no. 26, pp. 2239–2242, 2009.

[57] M. Ahmad, S. Al-Hawat, M. Akel, and O. Mrad, "Characterization of bismuth nanospheres deposited by plasma focus device," *Journal of Applied Physics*, vol. 117, no. 6, p. 063301, 2015.

[58] D. Ma, J. Zhao, Y. ZhaoXiao et al., "Synthesis of bismuth nanoparticles and self-assembled nanobelts by a simple aqueous route in basic solution," *Colloids and Surfaces A: Physicochemical and Engineering Aspects*, vol. 395, pp. 276–283, 2012.

[59] M. Tian, J. Wang, Q. Zhang et al., "Superconductivity and quantum oscillations in crystalline Bi nanowire," *Nano Letters*, vol. 9, no. 9, pp. 3196–3202, 2009.

[60] J. Kim, W. Shim, and W. Lee, "Bismuth nanowire thermoelectrics," *Journal of Materials Chemistry C*, vol. 3, no. 46, pp. 11999–12013, 2015.

[61] G. Chun-Lei, D. Qian, C.-H. Liu, J.-F. Jia, and F. Liu, "Topological edge states and electronic structures of a 2D topological insulator: single-bilayer Bi (111)," *Chinese Physics B*, vol. 22, no. 6, p. 067304, 2013.

[62] M. Tian, J. Wang, N. Kumar et al., "Observation of superconductivity in granular Bi nanowires fabricated by

electrodeposition," *Nano Letters*, vol. 6, no. 12, pp. 2773–2780, 2006.

[63] J. Toudert, R. Serna, and M. Jiménez de Castro, "Exploring the optical potential of nano-bismuth: tunable surface plasmon resonances in the near ultraviolet-to-near infrared range," *Journal of Physical Chemistry C*, vol. 116, no. 38, pp. 20530–20539, 2012.

[64] Y. Tian, L. Jiang, Y. Deng, S. Deng, G. Zhang, and X. Zhang, "Bi-nanorod/Si-nanodot hybrid structure: surface dewetting induced growth and its tunable surface plasmon resonance," *Optical Materials Express*, vol. 5, no. 11, pp. 2655–2666, 2015.

[65] E. Shapira, A. Holtzman, D. Marchak, and Y. Selzer, "Very high thermopower of Bi nanowires with embedded quantum point contacts," *Nano Letters*, vol. 12, no. 2, pp. 808–812, 2012.

[66] Y. M. Lin, S. B. Cronin, J. Y. Ying, M. S. Dresselhaus, and J. P. Heremans, "Transport properties of Bi nanowire arrays," *Applied Physics Letters*, vol. 76, no. 26, pp. 3944–3946, 2000.

[67] L. Li, Y. Zhang, G. Li, and L. Zhang, "A route to fabricate single crystalline bismuth nanowire arrays with different diameters," *Chemical Physics Letters*, vol. 378, no. 3, pp. 244–249, 2003.

[68] M. R. Black, Y.-M. Lin, S. B. Cronin, O. Rabin, and M. S. Dresselhaus, "Infrared absorption in bismuth nanowires resulting from quantum confinement," *Physical Review B*, vol. 65, no. 19, p. 195417, 2002.

[69] M. Murata and Y. Hasegawa, "Focused ion beam processing to fabricate ohmic contact electrodes on a bismuth nanowire for Hall measurements," *Nanoscale Research Letters*, vol. 8, no. 1, p. 400, 2013.

[70] A. Nikolaeva, T. E. Huber, D. Gitsu, and L. Konopko, "Diameter-dependent thermopower of bismuth nanowires," *Physical Review B*, vol. 77, no. 3, p. 035422, 2008.

[71] Y. T. Cheng, A. M. Weiner, C. A. Wong, M. P. Balogh, and M. J. Lukitsch, "Stress-induced growth of bismuth nanowires," *Applied Physics Letters*, vol. 81, no. 17, pp. 3248–3250, 2002.

[72] D. Su, S. Dou, and G. Wang, "Bismuth: a new anode for the Na-ion battery," *Nano Energy*, vol. 12, pp. 88–95, 2015.

[73] W. Z. Wang, B. Poudel, Y. Ma, and Z. F. Ren, "Shape control of single crystalline bismuth nanostructures," *Journal of Physical Chemistry B*, vol. 110, no. 51, pp. 25702–25706, 2006.

[74] A. Boukai, K. Xu, and J. R. Heath, "Size-dependent transport and thermoelectric properties of individual polycrystalline bismuth nanowires," *Advanced Materials*, vol. 18, no. 7, pp. 864–869, 2006.

[75] Z. Zhang, J. Y. Ying, and M. S. Dresselhaus, "Bismuth quantum-wire arrays fabricated by a vacuum melting and pressure injection process," *Journal of Materials Research*, vol. 13, no. 7, pp. 1745–1748, 1998.

[76] L. Li, Y. W. Yang, X. H. Huang, G. H. Li, R. Ang, and L. D. Zhang, "Fabrication and electronic transport properties of Bi nanotube arrays," *Applied Physics Letters*, vol. 88, no. 10, p. 103119, 2006.

[77] J. Heremans, C. M. Thrush, Z. Zhang et al., "Magnetoresistance of bismuth nanowire arrays: a possible transition from one-dimensional to three-dimensional localization," *Physical Review B*, vol. 58, no. 16, p. R10091, 1998.

[78] Z. Zhang, D. Gekhtman, M. S. Dresselhaus, and J. Y. Ying, "Processing and characterization of single-crystalline ultrafine bismuth nanowires," *Chemistry of Materials*, vol. 11, no. 7, pp. 1659–1665, 1999.

[79] C. M. Smith, N. Venkataraman, M. T. Gallagher et al., "Low-loss hollow-core silica/air photonic bandgap fibre," *Nature*, vol. 424, no. 6949, p. 657, 2003.

[80] M. Murata, Y. Hasegawa, T. Komine, and T. Kobayashi, "Preparation of bismuth nanowire encased in quartz template for Hall measurements using focused ion beam processing," *Nanoscale Research Letters*, vol. 7, no. 1, p. 505, 2012.

[81] Y. W. Park, H-J. Jung, and S.-G. Yoon, "Bi_2O_3 nanowire growth from high-density Bi nanowires grown at a low temperature using aluminum–bismuth co-deposited films," *Sensors and Actuators B: Chemical*, vol. 156, no. 2, pp. 709–714, 2011.

[82] V. V. Volobuev, P. Dziawa, A. N. Stetsenko et al., "The mechanism of Bi nanowire growth from Bi/Co immiscible composite thin films," *Journal of Nanoscience and Nanotechnology*, vol. 12, no. 11, pp. 8624–8629, 2012.

[83] J. Ham, J. Kang, J.-S. Noh, and W. Lee, "Self-assembled Bi interconnections produced by on-film formation of nanowires for in situ device fabrication," *Nanotechnology*, vol. 21, no. 16, p. 165302, 2010.

[84] J. Ham, W. Shim, D. H. Kim et al., "Direct growth of compound semiconductor nanowires by on-film formation of nanowires: bismuth telluride," *Nano Letters*, vol. 9, no. 8, pp. 2867–2872, 2009.

[85] S. Cao, C. Guo, Y. Wang, J. Miao, Z. Zhang, and Q. Liu, "Transparency conversion mechanism and laser induced fast response of bimetallic Bi/In thin film," in *Proceedings of SPIE, The International Society for Optical Engineering*, Society of Photo-ptical Instrumentation Engineers, Bellingham, WA, USA, 2008.

[86] V. T. Volkov, A. Y. Kasumov, Y. A. Kasumov, and I. I. Khodos, "Formation and possible growth mechanism of bismuth nanowires on various substrates," *Applied Physics A*, vol. 123, no. 8, p. 503, 2017.

[87] B. K. Wu, H.-Y. Lee, and M.-Y. Chern, "Bismuth nanowire grown naturally using a sputtering system," *Applied Physics Express*, vol. 6, no. 3, p. 035504, 2013.

[88] S. Cao, C. Guo, Y. Wang, J. Miao, Z. Zhang, and Q. Liu, "Template-catalyst-free growth of single crystalline bismuth nanorods by RF magnetron sputtering method," *Solid State Communications*, vol. 149, no. 1, pp. 87–90, 2009.

[89] J. Zhao, Q. Han, J. Zhu, X. Wu, and X, Wang, "Synthesis of Bi nanowire networks and their superior photocatalytic activity for Cr(vi) reduction," *Nanoscale*, vol. 6, no. 17, pp. 10062–10070, 2014.

[90] B. Lavinia, R. Schneider, D. Billaud, Y. Fort, and J. Ghanbaja, "A new synthesis of ultrafine nanometre-sized bismuth particles," *Nanotechnology*, vol. 15, no. 8, p. 940, 2004.

[91] Y. Wang and K. S. Kim, "Large-scale polyol synthesis of single-crystal bismuth nanowires and the role of NaOH in the synthesis process," *Nanotechnology*, vol. 19, no. 26, p. 265303, 2008.

[92] D. McCarthy and S. Brown, "Anisotropic corner crossing barriers in nanorod growth," *Journal of Physics: Conference Series*, vol. 100, no. 7, p. 072007, 2008.

[93] J. M. McMahon, G. C. Schatz, and S. K. Gray, "Plasmonics in the ultraviolet with the poor metals Al, Ga, In, Sn, Tl, Pb, and Bi," *Physical Chemistry Chemical Physics*, vol. 15, p. 5415, 2013.

[94] X. Chang, L. Xie, W. E. I. Sha et al., "Probing the light harvesting and charge rectification of bismuth nanoparticles behind the promoted photoreactivity onto Bi/BiOCl catalyst

by (in-situ) electron microscopy," *Applied Catalysis B: Environmental*, vol. 201, pp. 495–502, 2017.

[95] Y. W. Wang, B. H. Hong, and K. S. Kim, "Size control of semimetal bismuth nanoparticles and the UV-Visible and IR absorption spectra," *Journal of Physical Chemistry B*, vol. 109, pp. 7067–7072, 2005.

[96] M. Jiménez de Castro, F. Cabello, J. Toudert et al., "Potential of bismuth nanoparticles embedded in a glass matrix for spectral-selective thermos-optical devices," *Applied Physics Letters*, vol. 105, p. 113102, 2014.

[97] G. Jiang, X. Li, M. Lan et al., "Monodisperse bismuth nanoparticles decorated graphitic carbon nitride: enhanced visible-light-response photocatalytic NO removal and reaction pathway," *Applied Catalysis B: Environmental*, vol. 205, pp. 532–540, 2017.

[98] Z. Jiao, M. Shang, J. Liu et al., "The charge transfer mechanism of Bi modified TiO_2 nanotube arrays: TiO_2 serving as a "charge transfer bridge," *Nano Energy*, vol. 31, pp. 96–104, 2017.

[99] M. Chen, Y. Li, Z. Wang et al., "Controllable synthesis of core-shell Bi@amorphous Bi_2O_3 nanospheres with tunable optical and photocatalytic activity for NO removal," *Industrial and Engineering Chemistry Research*, vol. 56, pp. 10251–10258, 2017.

[100] S. Sivaramakrishnan, V. S. Muthukumar, S. Sivasankara Sai et al., "Nonlinear optical scattering and absorption in bismuth nanorod suspensions," *Applied Physics Letters*, vol. 91, no. 9, p. 093104, 2007.

[101] Y. Zhou, W. Li, Q. Zhang et al., "Non-noble metal plasmonic photocatalysis in semimetal bismuth films for photocatalytic NO oxidation," *Physical Chemistry Chemical Physics*, vol. 19, p. 25610, 2017.

[102] X. Li, Y. Sun, T. Xiong et al., "Activation of amorphous bismuth oxide via plasmonic Bi metal for efficient visible-light photocatalysis," *Journal of Catalysis*, vol. 352, pp. 102–112, 2017.

[103] Y. Gao, Y. Huang, Y. Li et al., "Plasmonic Bi/$ZnWO_4$ microspheres with improved photocatalytic activity on NO removal under visible light," *ACS Sustainable Chemistry and Engineering*, vol. 4, pp. 6912–6920, 2016.

[104] F. Dong, T. Xiong, S. Yan et al., "Facets and defects cooperatively promote visible light plasmonic photocatalysis with Bi nanowires@BiOCl nanosheets," *Journal of Catalysis*, vol. 344, pp. 401–410, 2016.

[105] F. Dong, Z. Zhao, Y. Sun et al., "An advanced semimetal-organic Bi spheres-g-C_3N_4 nanohybrid with SPR-enhanced visible-light photocatalytic performance for NO purification," *Environmental Science and Technology*, vol. 49, pp. 12432–12440, 2015.

[106] Y. Chen, D. Chen, J. Chen et al., "Facile synthesis of Bi nanoparticle modified with TiO_2 with enhanced visible light photocatalytic activity," *Journal of Alloys and Compounds*, vol. 651, pp. 114–120, 2015.

[107] C. A. Hoffman, J. R. Meyer, F. J. Bartoli et al., "Semimetal-to-semiconductor transition in bismuth thin films," *Physical Review B*, vol. 48, p. 11431, 1993.

[108] B.-K. Wu, M.-Y. Chern, and H.-T. Lee, "Size-controllable synthesis and bandgap modulation of single-layered RF-sputtered bismuth nanoparticles," *Nanoscale Research Letters*, vol. 9, p. 249, 2014.

[109] D. Velasco-Arias, I. Zumeta-Dubé, D. Díaz et al., "Stabilization of strong quantum confined colloidal bismuth nanoparticles, one-pot synthesized at room temperature," *Journal of Physical Chemistry C*, vol. 116, no. 27, pp. 14717–14727, 2012.

[110] N. Jiang, D. Su, J. C. H. Spence, S. Zhou, and J. Qiu, "Volume plasmon of bismuth nanoparticles," *Solid State Communications*, vol. 149, no. 3-4, pp. 111–114, 2009.

[111] M. S. Sander, R. Gronsky, Y. M. Lin, and M. S. Dresselhaus, "Plasmon excitation modes in nanowire arrays," *Journal of Applied Physics*, vol. 59, no. 5, p. 2733, 2001.

[112] M. R. Black, M. Padi, S. B. Cronin et al., "Intersubband transitions in bismuth nanowires," *Applied Physics Letters*, vol. 77, p. 4142, 2000.

[113] T. W. Cornelius, M. E. Toimil-Molares, and R. Neumann, "Quantum size effects manifest in infrared spectra of single bismuth nanowires," *Applied Physics Letters*, vol. 88, p. 103114, 2006.

[114] F. Khalilzadeh-Rezaie, C. W. Smith, J. Nath et al., "Infrared surface polaritons on bismuth," *Journal of Nanophotonics*, vol. 9, no. 093792, 2015.

[115] J. W. Cleary, G. Medhi, M. Shahzad et al., "Infrared surface plasmon resonance biosensor," in *Proceedings of SPIE 767306*, Moscow, Russia, 2010.

[116] R. Márquez-Islas, B. Zenteno-Mateo, B. Flores-Desirena et al., "Plasma-phonon polaritons in superlattices of semimetal bismuth and polaritonic material," *Optical Materials Express*, vol. 5, no. 12, p. 28020, 2015.

[117] Y. Li, Y. Zhao, and J. Zhao, "Facile and efficient synthesis of bismuth nanowires for improved photocatalytic activity," *Inorganic Chemistry*, vol. 55, pp. 4897–4905, 2016.

[118] L. Yan, Z. Gu, X. Zheng et al., "Elemental bismuth-graphene heterostructures for photocatalysis from ultraviolet to infrared light," *ACS Catalysis*, vol. 7, pp. 7043–7050, 2017.

[119] Y. Sun, Z. Zhao, W. Zhang et al., "Plasmonic Bi metal as cocatalyst and photocatalyst: the case of Bi/$(BiO)_2CO_3$ and Bi particles," *Journal of Colloid and Interface Science*, vol. 485, pp. 1–10, 2017.

[120] T. Xiong, X. Dong, H. Huang et al., "Single precursor mediated-synthesis of Bi semimetal deposited N-doped $(BiO)_2CO_3$ superstructures for highly promoted photocatalysis," *ACS Sustainable Chemistry and Engineering*, vol. 4, pp. 2969–2979, 2016.

[121] F. Dong, Q. Li, Y. Sun, and W.-K. Ho, "Noble metal-like behavior of plasmonic Bi particles as a cocatalyst deposited on $(BiO_2)CO_3$ microspheres for efficient visible light photocatalysis," *ACS Catalysis*, vol. 4, pp. 4341–4350, 2014.

[122] Y. Sun, Z. Zhao, F. Dong, and W. Zhang, "Mechanism of visible light photocatalytic NOx oxidation with plasmonic Bi cocatalyst-enhanced $(BiO_2)CO_3$ hierarchical microspheres," *Physical Chemistry Chemical Physics*, vol. 17, pp. 10383–10390, 2015.

[123] N. A. Kouamé, O. T. Alaoui, A. Herissan et al., "Visible light-induced photocatalytic activity of modified titanium(iv) oxide with zero-valent bismuth clusters," *New Journal of Chemistry*, vol. 39, no. 3, pp. 2316–2322, 2015.

[124] J. Xiao, W. Yang, and Q. Li, "Bi quantum dots on rutile TiO2 as hole trapping centers for efficients photocatalytic bromate reduction under visible light illumination," *Applied Catalysis B: Environmental*, vol. 218, pp. 111–118, 2017.

[125] P. Kar, T. K. Maji, R. Nandi, P. Lemmens, and S. K. Pal, "In-situ hydrothermal synthesis of Bi-$Bi_2O_2CO_3$ heterojunction photocatalyst with enhanced visible light photocatalytic activity," *Nano-Micro Letters*, vol. 9, no. 2, p. 18, 2017.

[126] L. Lu, W. Wang, L. Wu et al., "All-optical switching of two continuous waves in few layer bismuthene based on spatial cross-phase modulation," *ACS Photonics*, vol. 4, no. 11, pp. 2852–2861, 2017.

[127] J. D. Yao, J. M. Shao, and G. W. Yang, "Ultra-broadband and high-responsive photodetectors based on bismuth film at room temperature," *Scientific Reports*, vol. 5, no. 1, p. 12320, 2015.

[128] J. Yao, Z. Zheng, J. Shao, and G. Yang, "Promoting photosensitivity and detectivity of the Bi/Si heterojunction photodetector by inserting a WS_2 layer," *Applied Materials and Interfaces*, vol. 7, no. 48, pp. 26701–26708, 2015.

[129] T. E. Huber, T. Brower, S. D. Johnson et al., "Photocurrent in bismuth junctions with graphene," arXiv:1709.05408, 2017.

[130] A. G. Bezerra Jr., P. Cavassin, T. N. Machado, T. D. Wolski, R. Caetano, and W. H. Schreiner, "Surface-enhanced Raman scattering using bismuth nanoparticles: a study with amino acids," *Journal of Nanoparticle Research*, vol. 19, p. 362, 2017.

[131] B. Wei, X. Zhang, C. Zhang et al., "Facile synthesis of uniform-sized bismuth nanoparticles for CT visualization of gastrointestinal tract in vivo," *ACS Applied Materials and Interfaces*, vol. 8, no. 20, pp. 12720–12726, 2016.

[132] X. Lu, A. Li, C. Zhao et al., "Ultrasmall semimetal nanoparticles of bismuth for dual-modal computed tomography/photoacoustic imaging and synergistic thermoradiotherapy," *ACS Nano*, vol. 11, no. 4, pp. 3990–4001, 2017.